

On the Convergence Theory of Pipeline Gradient-based Analog In-memory Training

Zhaoxian Wu, Quan Xiao, Tayfun Gokmen, Hsinyu Tsai, Kaoutar El Maghraoui,

Tianyi Chen

Abstract

Aiming to accelerate the training of large deep neural networks (DNN) in an energy-efficient way, analog in-memory computing (AIMC) emerges as a solution with immense potential. AIMC accelerator keeps model weights in memory without moving them from memory to processors during training, reducing overhead dramatically. Despite its efficiency, scaling up AIMC systems presents significant challenges. Since weight copying is expensive and inaccurate, data parallelism is less efficient on AIMC accelerators. It necessitates the exploration of pipeline parallelism, particularly asynchronous pipeline parallelism, which utilizes all available accelerators during the training process. This paper examines the convergence theory of stochastic gradient descent on AIMC hardware with an asynchronous pipeline (*Analog-SGD-AP*). Although there is empirical exploration of AIMC accelerators, the theoretical understanding of how analog hardware imperfections in weight updates affect the training of multi-layer DNN models remains underexplored. Furthermore, the asynchronous pipeline parallelism results in stale weights issues, which render the update signals no longer valid gradients. To close the gap, this paper investigates the convergence properties of *Analog-SGD-AP* on multi-layer DNN training. We show that the *Analog-SGD-AP* converges with iteration complexity $\mathcal{O}(\varepsilon^{-2} + \varepsilon^{-1})$ despite the aforementioned issues, which matches the complexities of digital SGD and Analog SGD with synchronous pipeline, except the non-dominant term $\mathcal{O}(\varepsilon^{-1})$. It implies that AIMC training benefits from asynchronous pipelining almost for free compared with the synchronous pipeline by overlapping computation.

Index Terms

Analog computing, in-memory computing, stochastic optimization, model parallelism

Z. Wu and Q. Xiao are with Cornell University, New York, NY 10044 ({zw868, qx232}@cornell.edu). T. Gokmen, H. Tsai, and K. El Maghraoui are with IBM Research, Yorktown Heights, NY 10598 ({tgokmen, htsai, kelmaghr}@us.ibm.com). T. Chen is with Rensselaer Polytechnic Institute and Cornell University (tianyi.chen@cornell.edu).

The work was done when the authors were at Rensselaer Polytechnic Institute. The work was supported by IBM through the IBM-Rensselaer Future of Computing Research Collaboration, the National Science Foundation Projects 2401297, 2532349, and 2532653, and by the Cisco Research Award.

I. INTRODUCTION

Deep Neural Networks (DNNs) have facilitated remarkable progress in a wide range of applications. As the model sizes and dataset volumes grow exponentially, DNN training and inference become time-consuming and resource-intensive. For example, training an LLAMA2 7B model requires 184 thousand GPU hours, and this increases to 1.7 million GPU hours for its 70B version [1]. In response to the escalating computational demands of large-scale DNN training and inference, the pursuit of specialized hardware accelerators has emerged. The ubiquitous fully connected and convolutional layers, whose core operation is matrix-vector multiplication (MVM), form the fundamental backbone of both training and inference as the demand for efficient processing intensifies. Typically, each forward and backward pass requires millions of multiply-accumulate (MAC) operations, necessitating specialized hardware with high performance and low energy consumption.

The promise of analog computing. To this end, a promising solution to accelerate the MVM operations is the *analog in-memory computing* (AIMC) accelerator, wherein both the input and output of the MVM operation are analog signals like current or voltage. The DNN weights are stored in analog crossbar tiles consisting of resistive elements [2] where the conductance of the resistive element represents the weight magnitude. Unlike traditional Von Neumann accelerators such as GPUs and TPUs, which move weights from memory to the processor during computation, AIMC accelerators keep the weights stationary and perform MVM operations in memory. Without moving weights frequently, AIMC accelerators enable time- and energy-

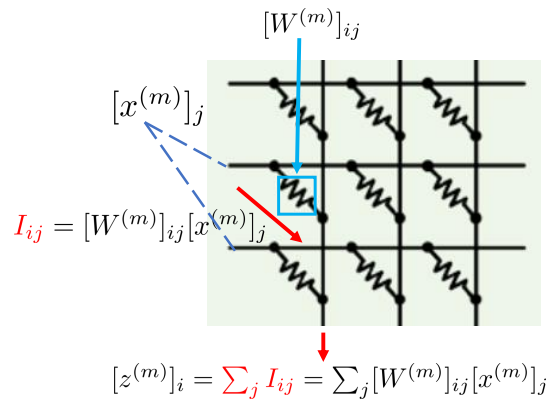


Fig. 1: Illustration of MVM computation in AIMC accelerators. The **weight** $W^{(m)}$ on layer m is stored in a crossbar tile. The (i, j) -th element of $W^{(m)}$ is represented by the **conductance** of the (i, j) -th resistive element. MVM operation $z^{(m)} = W^{(m)}x^{(m)}$ is performed by applying **voltage** $[x^{(m)}]_j$ between j -th and $(j + 1)$ -th row. By Ohm's law, the **current** is $I_{ij} = [W^{(m)}]_{ij} [x^{(m)}]_j$; and by Kirchhoff's law, the total current on the i -th column is $\sum_j I_{ij} = \sum_j [W^{(m)}]_{ij} [x^{(m)}]_j$. Unlike the digital counterpart, no movement of $W^{(m)}$ is required for MVM calculation.

efficient MVM computations; see Fig. 1.

The curse of data parallelism. While efficient computation is beneficial, in-memory computing imposes scalability limitations. Specifically, contemporary DNN optimizers depend on mini-batch SGD to facilitate highly parallel training. In the Von Neumann computation architecture, the most efficient parallel mechanism is *data parallelism* [3], where DNN weights are replicated to different accelerators to support gradient descent with large batches [4, 5]. By contrast, in the AIMC architecture, trainable weights are stored in the analog tiles as the conductances of resistive elements; thus, copying weights is expensive and prone to error. Therefore, data parallelism, the enabling factor of large-scale AI training, is unrealistic for AIMC accelerators.

Due to the physical limitations on the AIMC accelerator, we instead resort to *pipeline parallelism* [6]. Pipeline parallelism partitions a large model into a series of stages distributed across multiple accelerators, with each stage corresponding to the computation of a few layers. After an accelerator processes one datum (or batch), it passes the intermediate outputs to the next accelerator and begins processing the next datum. Pipeline parallelism overlaps computation across different accelerators, increasing system throughput.

Synchronous and asynchronous parallelism. As the requirement of training large models emerges, a plethora of pipeline parallel libraries have been developed, including Gpipe [7, 8], Deepspeed [9], FSDP [10], Megetron-LM [11], Colossal-AI [12], just to name a few. In their implementation, a gradient *mini-batch* (e.g., with batch size 128) is split into *micro-batches* (e.g., 8 micro-batches with batch size 16) and filled into the pipeline. The model weights are updated after all the micro-batches are processed. Featuring the synchronization operation at the end of each mini-batch, this pipeline paradigm is referred to as *synchronous pipeline*. However, during the fill and drain phases, the pipeline is not fully occupied, which limits the device utilization. To overcome the issue, *asynchronous pipeline* is proposed, which continuously fills the micro-batch into the pipeline and updates the weights once the gradient is available. Asynchronous pipeline increases the device utilization, while the weights for gradient computing can be stale, leading to a biased training dynamic.

To fully realize the promise of analog training, this paper focuses on the theoretical under-

standing of the viability of stochastic gradient descent on AIMC hardware with asynchronous pipeline (Analog-SGD-AP). Besides the stale signal issue in the asynchronous pipeline, the update dynamics on AIMC accelerators also suffer from bias since the weight update involves adjusting conductance, which is difficult to control in theory. Both stale signals and imperfect update dynamics lead to the following natural question:

How do their combined effects provably impact training on the AIMC accelerator?

Despite two sources of bias, this paper theoretically demonstrates that Analog-SGD-AP converges at almost the same rate as SGD on a single AIMC accelerator (Analog-SGD-WOP) and SGD on AIMC hardware with synchronous pipeline (Analog-SGD-SP), providing a theoretical foundation for parallel AIMC training.

A. Main results

This paper aims to understand the impact of bias and investigate the computational complexities and acceleration effect of Analog-SGD-AP. We highlight the unique technical challenges compared with the analysis of the asynchronous pipeline on digital accelerators as follows.

T1) Unlike the digital training with precise weight update, the update dynamics on AIMC accelerators include an asymmetric bias. To be specific, consider an analog weight W_k on a resistive crossbar array and a desired update ΔW_k . The updated weight becomes

$$\text{Analog Update} \quad W_{k+1} = W_k + \Delta W_k - \frac{1}{\tau} |\Delta W_k| \odot W_k^{(m)} \quad (1)$$

where τ is a hardware-specific constant, $|\cdot|$ is element-wise absolute value, and \odot is the element-wise production. Unlike the accurate digital training, the last bias term in (1) is unique to analog accelerators. This bias can not be eliminated within a reasonable cost and leads to challenges to the analysis. In section II-B, we provide more background.

T2) Even though there are already theoretical works on the design of the asynchronous pipeline, most of them model it as a delayed gradient method [13]. However, in the asynchronous pipeline, the forward pass is performed using stale weights, while the backward pass uses

Pipeline Type	Sample Complexity	Comp. Density	Wall-clock Complexity
Analog-SGD-WOP	$\mathcal{O}(\sigma^2 \varepsilon^{-2})$	$\frac{1}{M}$	$\mathcal{O}(M \sigma^2 \varepsilon^{-2})$
Analog-SGD-SP [Thm. 1]	$\mathcal{O}(\sigma^2 \varepsilon^{-2})$	$\frac{B}{M+B-1}$	$\mathcal{O}((M+B)B^{-1} \sigma^2 \varepsilon^{-2})$
Analog-SGD-AP [Thm. 2]	$\mathcal{O}(\sigma^2 \varepsilon^{-2} + \varepsilon^{-1})$	1	$\mathcal{O}(\sigma^2 \varepsilon^{-2} + \varepsilon^{-1})$

TABLE I: Comparison of different pipeline strategies. Sample complexity is the number of samples needed to achieve a training loss $\leq \varepsilon$. Computing density is the average portion of active accelerators. In the table, M and B are the number of stages and micro-batches, respectively. Wall-clock complexity measures the running time for achieving training loss $\leq \varepsilon$, which in math is sample complexity divided by computation density.

the latest weights. Consequently, their inconsistent multiplication used for weight updates is not a valid gradient, and this error accumulates during training. The stale signals in DNN render the update increment used in Analog-SGD-AP no longer a valid gradient, making its convergence behavior unclear.

T3) Multi-layer DNN models accumulate error through layers, leading to challenges in the analysis. Without considering a specific multi-layer architecture, prior work [14] treats all weights as a whole, thereby failing to capture the multi-layer DNN structure.

Overcoming the challenges, this paper answers the question above and provides both a convergence guarantee and computational complexities. The key contributions are as follows.

C1) We consider the training of a multi-layer DNN, which consists of linear layers and non-linear activation functions. We formulate the training dynamics of Analog-SGD-AP, which reflects the stale weights in the asynchronous pipeline and the bias from the AIMC accelerators' imperfection. We investigate the smoothness of the training objective as well as the robustness of the network against stale weights.

C2) We analyze three types of computation complexities of the asynchronous pipeline training in AIMC accelerators: iteration, sample, and wall-clock complexities. The crucial step is to construct a Lyapunov function that has sufficient descents at each iteration. We show that Analog-SGD-AP has the sample complexity $\mathcal{O}(\sigma^2 \varepsilon^{-2} + \varepsilon^{-1})$, which is the same as that of Analog-SGD-WOP and Analog-SGD-SP except for the higher-order term $\mathcal{O}(\varepsilon^{-1})$. Unlike the synchronous pipeline, the asynchronous pipeline utilizes all available accelerators and increases the computation density from $\frac{B}{M+B-1}$ to 1, where B is the number of micro-

batches and M is the number of stages. For example, $M = 4$ and $B = 4$ lead to about $1.7\times$ computation density. The results are summarized in Table I.

C3) We verify the speedup of Analog-SGD-AP against Analog-SGD-WOP and Analog-SGD-SP in AIMC accelerator simulator, AIHWKIT. Numerical simulation results show that despite a slightly larger sample complexity, Analog-SGD-AP achieves the same accuracy with fewer clock cycles due to its high computation density, which is consistent with the theoretical guarantee. Furthermore, empirical results show that Analog-SGD-AP achieves linear speedup at least within the range of 1-8 accelerators.

B. Prior art.

To put our work in context, we review prior art that we group into the following two categories. **Gradient-based training on AIMC accelerators.** Analog training has shown promising early successes in certain tasks [15–17], and a series of analog-friendly algorithms has been proposed to enable the gradient-based on-chip training on the AIMC hardware. However, the asymmetric update and noisy gradient lead to large asymptotic errors in training [18]. Numerous algorithms have been proposed to address these issues. TT-v1 [19] heuristically introduces an auxiliary analog array as a gradient approximation to eliminate the asymptotic error. To demonstrate its efficiency, [20] establishes a model to characterize the dynamics of the analog training and provides a theoretical convergence guarantee. Building on that, [21] investigates the impact of response functions on the training and demonstrates how its impact can be alleviated by bilevel optimization methods. To filter out the high-frequency noise introduced by inter-device transfer, TT-v2 [22] introduces a digital array. Based on TT-v1/v2, Chopped-TTv2 (c-TTv2) and Analog Gradient Accumulation with Dynamic reference (AGAD) [23] are proposed to mitigate the impact of inaccurate symmetric point correction [24]. To overcome the limit update granularity issue, [25] proposed a multi-tile training paradigm. However, the mentioned works focus on training single AIMC accelerators. Instead, this work aims to scale up the system by parallelizing model computation.

Asynchronous pipeline. Existing works proposed methods to alleviate the stale weight issues in the asynchronous pipeline. For instance, [26] proposed weight-prediction approaches to com-

pensate for the delay, PipeDream [27] combined the synchronous and asynchronous pipeline parallelisms to achieve greater speedup; and [28] and [29] propose only overlapping gradient computation and communication to ensure the delay is one. These algorithms are *not for analog pipeline training*. Researchers also attempted to design analog pipeline circuits to accelerate the training [30, 31], but they focus on the synchronous pipeline. On the theory side, there are few studies on pipeline training for digital accelerators such as [14, 32], but their algorithms either require weight stashing, which is *expensive for analog accelerators*, or slow down digital SGD through higher-order terms. As [27] points out, delay affects both forward and backward passes in the asynchronous pipeline DNN training, rendering the increment no longer a valid gradient and making the analysis challenging.

II. ANALOG TRAINING WITH MODEL PARALLELISM

In this section, we first introduce the multi-layer DNN training model, and then introduce the analog stochastic gradient descent algorithm with the asynchronous pipeline.

A. Training problem and back-propagation

Consider a standard model training problem on a data distribution \mathcal{P} given by

$$\min_{W \in \mathbb{R}^D} \left\{ f(W) := \mathbb{E}_{\xi \sim \mathcal{P}} [f(W; \xi)] \right\} \quad (2)$$

where W is the trainable model weights on analog crossbar tiles, which is vectorized into a D -dimension vector.

DNN model. Consider the multi-layer DNN, which consists only of linear layers and activation functions. Let $[M] := \{1, 2, \dots, M\}$ denote an index set. The trainable weights are separated into M different blocks, i.e., $W = [W^{(1)}, W^{(2)}, \dots, W^{(M)}]$, where $W^{(m)}, \forall m \in [M]$ is a matrix. The training of DNN typically consists of three phases: forward, backward, and update. Suppose x and y are the feature and label of data $\xi = (x, y) \in \mathcal{X} \times \mathcal{Y}$, where \mathcal{X} and \mathcal{Y} are feature and label spaces, respectively. The forward pass of the model for layer $m \in [M]$ is expressed by

$$\text{Forward} \quad x^{(1)} = x, \quad z^{(m)} = W^{(m)}x^{(m)}, \quad x^{(m+1)} = g^{(m)}(z^{(m)}) \quad (3)$$

where $g^{(m)}(\cdot)$ is the activation function of layer m , and $x^{(m)}$ is the input feature. At the last layer, the output $x^{(M)}$ and label y are fed together into the loss function $\ell(\cdot, \cdot) : \mathcal{Y} \times \mathcal{Y} \rightarrow \mathbb{R}$ and yields $f(W; \xi) = \ell(x^{(M+1)}, y)$. For the backward pass, define the backward signal $\delta^{(m)} := \frac{\partial f(W; \xi)}{\partial z^{(m)}}$, wherein the error of the last layer is first computed by $\delta^{(M)} = \nabla_{x^{(M+1)}} \ell(x^{(M+1)}, y) \nabla g^{(M)}(z^{(M)})$. Subsequently, each layer $m \in [M - 1]$ computes the next recursion by the chain rule

$$\text{Backward} \quad \delta^{(m)} = \frac{\partial f(W; \xi)}{\partial z^{(m+1)}} \frac{\partial z^{(m+1)}}{\partial x^{(m+1)}} \frac{\partial x^{(m+1)}}{\partial z^{(m)}} = (\delta^{(m+1)} W^{(m)}) \nabla g^{(m)}(z^{(m)}). \quad (4)$$

In the forward pass, the activation $z^{(m)}$ is stashed until the backward signal $\delta^{(m+1)}$ returns. Typically, the computation $\nabla g^{(m)}(z)$ is light-weight, and hence the major overhead of the backward pass lies at the MVM among $W^{(m)}$ and $\delta^{(m)}$. With the forward and backward signals, the gradient with respect to the weight $W^{(m)}$ of layer m is computed by

$$\text{Gradient} \quad \nabla_{W^{(m)}} f(W; \xi) = \frac{\partial f(W; \xi)}{\partial z^{(m)}} \frac{\partial z^{(m)}}{\partial W^{(m)}} = \delta^{(m)} \otimes x^{(m)} \quad (5)$$

where \otimes is the outer product between two vectors.

Rank-update Unlike digital accelerators, AIMC accelerators use *rank-update* to change the matrix, which leverages the outer product structure as shown in (5). To do so, independent random voltage pulses with probability proportional to the elements of $\delta^{(m)}$ and $x^{(m)}$ are applied to columns and rows, respectively. Consequently, the (i, j) -th element $[W]_{i,j}$ receives a pulse coincident with probability $\propto [\delta^{(m)}]_i [x^{(m)}]_j$. Without computing the whole matrix $\delta^{(m)} \otimes x^{(m)}$ explicitly, rank-update has only $O(BN)$ complexity while the update on digital accelerators has $O(BN^2)$ complexity to update an $N \times N$ matrix. Consequently, AIMC accelerators perform the update operation in a fast and energy-efficient way [15].

B. Non-ideal update on AIMC accelerator

Despite the ultra-efficient weight update on the AIMC accelerator, as noted by [19–21], the update on AIMC accelerators exhibits asymmetric bias. To be specific, for any desired update $\Delta W_k^{(m)}$, the update on W_k is scaled by response functions $q_+(\cdot)$ and $q_-(\cdot)$. Considering the

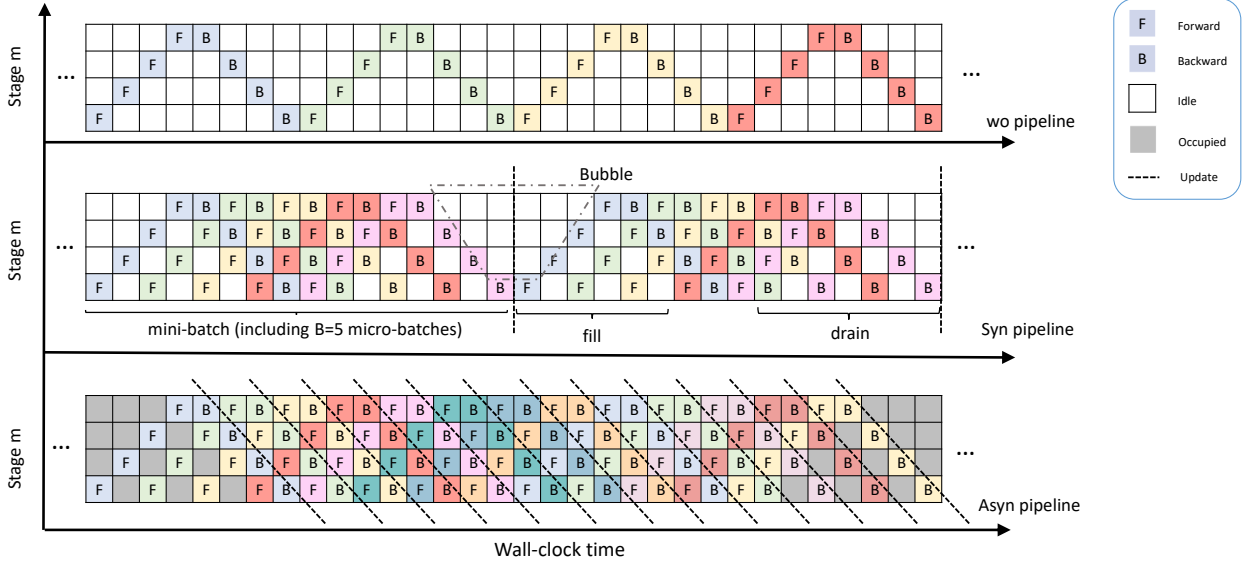


Fig. 2: Illustration of pipelines with 4 accelerators ($M = 4$). Each mini-batch is split into $B = 4$ micro-batches. Each color represents one micro-batch, and each row from bottom to top represents stages 0 to 4. Each column corresponds to a single clock cycle in which one micro-batch is processed. The white square indicates the corresponding accelerator is idle. **(Top)** Analog-SGD-WOP. All weights are updated after each mini-batch is computed, which is not presented in the figure. **(Middle)** Analog-SGD-SP with micro-batch count $B = 5$. The update occurs after all 5 micro-batches are processed. **(Bottom)** Analog-SGD-AP. The update occurs once the gradient of a single micro-batch is achieved. The grey square indicates that the corresponding accelerator is processing data that is not fully reflected in the figure.

weight W_k at iteration k and the expected update $\Delta W \in \mathbb{R}^D$, we express the asymmetric update as $W_{k+1} = U(W_k, \Delta W)$ with the update function $U : \mathbb{R} \times \mathbb{R} \rightarrow \mathbb{R}$ defined by

$$U(w, \Delta w) := \begin{cases} w + \Delta w \cdot q_+(w), & \Delta w \geq 0, \\ w + \Delta w \cdot q_-(w), & \Delta w < 0. \end{cases} \quad (6)$$

Defining the symmetric and asymmetric components as $F(w) := \frac{1}{2}(q_-(w) + q_+(w))$ and $G(w) := \frac{1}{2}(q_-(w) - q_+(w))$, we write the update in (6) as $U(w, \Delta w) = w + \Delta w \cdot F(w) - |\Delta w| \cdot G(w)$.

This paper consider a special case that $q_+(w) = 1 - w/\tau$, $q_-(w) = 1 + w/\tau$ as suggested by [20], we reach the dynamics (1).

C. Synchronous and asynchronous pipelines

Consider training a large model using a mini-batch size B_{mini} , which is too large to fit into one accelerator and necessitates *model parallelism*. In model parallelism, the forward and

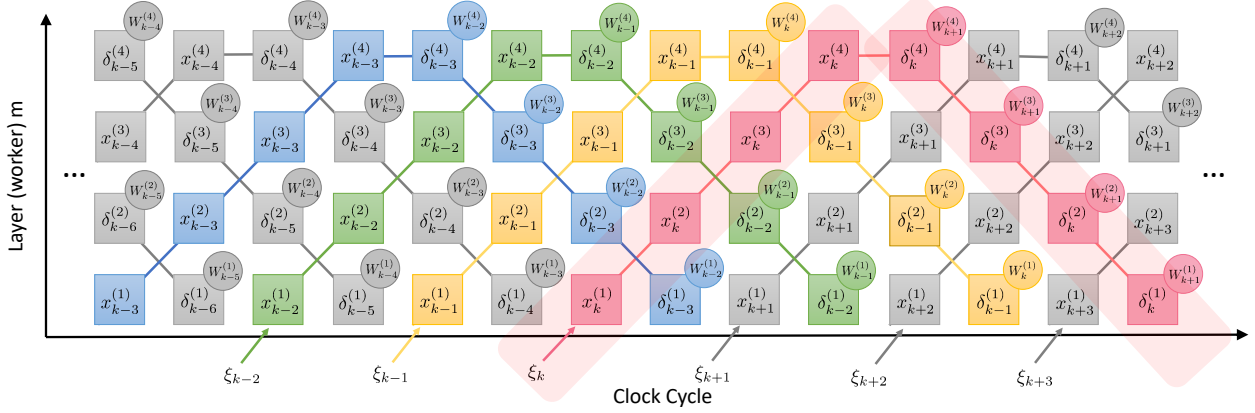


Fig. 3: Illustration of the dynamics of the asynchronous pipeline. The $W_k^{(m)}$ in the circle implies the update happens in this clock cycle, and the symbols in the squares indicate the input of each accelerator.

backward computations are partitioned into a sequence of *stages*, which, in general, consist of a consecutive set of layers in the model. Each stage is mapped to one digital or analog accelerator. Apart from the model separation, a mini-batch of data is also split into B *micro-batch* of size $B_{\text{micro}} := B_{\text{mini}}/B$. Without loss of generality, this paper assumes that one stage contains only one layer and the micro-batch size $B_{\text{micro}} = 1$. Under this assumption, $\xi_{k,b}$ denotes the b -th micro-batch which contains only the b -th data. Consequently, the number of micro-batches is the mini-batch size, i.e., $B = B_{\text{mini}}$. This paper treats a stage as the minimal scheduling unit and investigates the time complexity across different scheduling strategies. To compare time costs, we define the basic time unit, *clock cycle*, as the minimum time required for all devices to process one micro-batch. Based on scheduling strategies, there are three types of model parallelism: vanilla model parallelism without pipelining, synchronous pipelining, and asynchronous pipelining. **Vanilla model parallelism without pipeline.** Let $\xi_{k,b}$, $b \in [B]$ denote the b -th micro-batch (containing only one data sample, as previously mentioned) for iteration k . Vanilla model parallelism processes micro-batches sequentially. In the forward pass, stage m achieves the output of the previous stage $x_{k,b}^{(m)}$ as input and outputs $x_{k,b}^{(m+1)}$ according to (3), while in the backward pass stage m achieves the backward signal $\delta_{k,b}^{(m)}$ from next stage and sends the error $\delta_{k,b}^{(m-1)}$ to its previous stage according to (4). The signals $x_{k,b}^{(m)}$ and $\delta_{k,b}^{(m)}$ are stashed when the gradient for the b -th micro-batch is completed. After achieving all $\{(x_{k,b}^{(m)}, \delta_{k,b}^{(m)}) : b \in [B_{\text{mini}}]\}$, the weights will be updated using the gradient-based method. Beginning from $W_{k,0} = W_k$, Analog

SGD update the weight as $W_{k+1}^{(m)} = W_{k,B}^{(m)}$, which iterates over $b \in [B_{\text{mini}}]$ by

$$W_{k,b+1}^{(m)} = W_{k,b}^{(m)} - \frac{\alpha}{B} \nabla_{W^{(m)}} f(W_k; \xi_{k,b}) - \frac{\alpha}{\tau B} |\nabla_{W^{(m)}} f(W_k; \xi_{k,b})| \odot W_{k,b}^{(m)}. \quad (7)$$

Notice that for digital SGD, the last term in the right-hand side (RHS) of (7) disappears, and hence (7) reduces to mini-batch SGD, i.e., $W_{k+1}^{(m)} = W_k^{(m)} - \frac{\alpha}{B} \sum_{b=1}^B \nabla_{W^{(m)}} f(W_k; \xi_{k,b})$. To fully release the potential of rank-update, AIMC accelerators follow (7) to update its weight, which in turn complicates the convergence analysis.

Synchronous pipeline. Vanilla model parallelism is simple to implement. However, most devices remain idle, reducing system throughput. Existing work has already attempted to design an architecture that supports the pipeline training [30, 31]. They faithfully implement the iteration (7) but overlap the computing inside a mini-batch. Featuring synchronization at the end of a mini-batch, this stage schedule mechanism is called *synchronous pipeline*. In the vanilla non-pipeline version, stage m remains idle after completing the forward computation of the b -th micro-batch until the backward signal returns from stage $m + 1$. In the synchronous pipelining, each stage sends the output signal $x_{k,b}^{(m+1)}$ to the next stage, while simultaneously starting to process the next forward signal $x_{k,b+1}^{(m)}$ or backward signal $\delta_{k,b-(M-m)}^{(m)}$, if any. Similar to the vanilla model parallelism, the weights will be updated after processing all micro-batches. Consequently, for each mini-batch, most of the devices need to wait until the last micro-batch is processed. After that, each device collects the gradients of the whole mini-batch and updates weights iteratively following (7). To implement that, a synchronization operation is required to wait for the completion of gradient computation before starting the next mini-batch. During the pipeline filling and draining periods, parts of the devices are idle; see the middle of Fig. 2

Asynchronous pipeline. To fully utilize all devices, a more progressive strategy, *asynchronous pipeline*, is proposed. Instead of using mini-batch descent, asynchronous pipeline performs gradient descent on each micro-batch. Let ξ_k denote the micro-batch for iteration k . In the forward pass, stage m receives the output of the previous stage $x_k^{(m)}$ as input and outputs $x_k^{(m+1)}$, while in the backward pass, stage m receives the backward signal $\delta_k^{(m)}$ from next stage and sends the error $\delta_k^{(m-1)}$ to its previous stage. Unlike the synchronous pipeline, the asynchronous

pipeline updates the weights once $x_k^{(m)}$ and $\delta_k^{(m)}$ are ready. Without regular synchronization and filling/draining period, no device is idle during the training, maximizing the utilization. See Fig. 2 for the comparison of different parallel computing strategies.

Despite its perfect resource usage, asynchronous pipeline parallelism suffers from the stale signal issue. Notice that in the asynchronous pipeline setting, the forward signal $x^{(m)}$ and backward signals $\delta^{(m)}$ are computed based on different stale weights. For example, after outputting forward signal $x^{(0)}$ for the k -th micro-batch, the first stage ($m = 1$) receives the backward signal $\delta^{(0)}$ after $2(M - 1)$ clock cycles, wherein $M - 1$ gradient updates happen. We introduce different symbols for precise description, which have tildes on top of them to indicate the staleness. Since there are $M - m$ gradient updates between the forward and backward passes in stage m , the weight used for the forward pass has a delay of $M - m$. In contrast, the weights are updated by the backward pass, which means the weights used for the backward pass are the latest ones. The forward and backward passes of asynchronous pipeline training can be summarized as

$$\text{Forward} \quad \tilde{x}_k^{(0)} = x_k, \quad \tilde{z}_k^{(m)} = W_{k-(M-m)}^{(m)} \tilde{x}_k^{(m)}, \quad \tilde{x}_k^{(m+1)} = g^{(m)}(\tilde{z}_k^{(m)}), \quad (8)$$

$$\text{Backward} \quad \tilde{\delta}_k^{(m)} = \tilde{\delta}_k^{(m+1)} W_k^{(m+1)} \nabla g^{(m)}(\tilde{z}_k^{(m)}). \quad (9)$$

Imperfect gradient-based training on AIMC accelerators. After getting the backward signal $\delta^{(m)}$, gradient-based algorithms can be used to update the weights. However, there is a bias due to the hardware imperfection [20]. Replacing ΔW_k with $-\alpha \tilde{\delta}_k^{(m)} \otimes \tilde{x}_k^{(m)}$ in (1), where $\alpha > 0$ is a positive learning rate, we reach the update dynamics of weights

$$\text{Update} \quad W_{k+1}^{(m)} = W_k^{(m)} - \alpha \tilde{\delta}_k^{(m)} \otimes \tilde{x}_k^{(m)} - \frac{\alpha}{\tau} |\tilde{\delta}_k^{(m)} \otimes \tilde{x}_k^{(m)}| \odot W_k^{(m)}. \quad (10)$$

In (10), the outer product $\tilde{\delta}_k^{(m)} \otimes \tilde{x}_k^{(m)}$ is not a valid gradient with respect to any weight $W^{(m)}$, which is referred to as partially stale gradient and makes the analysis more challenging.

The main challenge coming from the AIMC training is the *weight drift* [20]. Consider the case where $W_k^{(m)}$ is already a non-zero critical point of $f(W)$ but not the one of $f(W; \xi)$, i.e.

$\mathbb{E}_{\xi \sim \mathcal{P}}[\nabla_{W^{(m)}} f(W_k^{(m)}; \xi)] = 0$ but $\nabla_{W^{(m)}} f(W_k^{(m)}; \xi) \neq 0$ for some ξ . After one iteration, the weight $W_k^{(m)}$ drifts because of the sample randomness

$$\mathbb{E}[W_{k+1}^{(m)}] - W_k^{(m)} = -\frac{\alpha}{\tau} \mathbb{E}[\|\nabla_{W^{(m)}} f(W_k^{(m)}; \xi)\|] \odot W_k^{(m)} \neq 0 \quad (11)$$

which prevents the weights from converging to the critical point, leading to an error.

III. CONVERGENCE & WALL-CLOCK ANALYSIS

This section shows that despite stale gradient issue and the update bias in AIMC accelerators, the asynchronous pipeline converges with the same sample complexity as the counterpart without pipeline or with synchronous pipeline. By increasing the computation density, asynchronous pipeline parallelism provides notable speedup in terms of wall-clock complexity.

A. Assumptions

Before showing the complexity of the pipeline algorithms, we first introduce a series of assumptions on the properties of DNN structures, data distribution, as well as the AIMC accelerators. $\|\cdot\|$ is ℓ_2 -norm for vectors and Frobenious norm for matrices; $\|\cdot\|_\infty$ takes the element with maximal absolute value of vector or matrix.

Assumption 1 (Unbiasness and bounded variance). *The stochastic gradient is unbiased and has bounded variance σ^2 .*

Assumption 2 (Normalized feature). *The feature is normalized, i.e. $\|x\| = 1, \forall x \in \mathcal{X}$.*

Assumption 3 (Activation function). *All activation function $g^{(m)}(\cdot)$, $m \in [M]$, is (i) Lipschitz continuous, i.e. $\|g^{(m)}(z) - g^{(m)}(z')\| \leq L_{g,0}\|z - z'\|$; (ii) smooth, i.e. $\|\nabla g^{(m)}(z) - \nabla g^{(m)}(z')\| \leq L_{g,1}\|z - z'\|$; (iii) centered, i.e. $g(0) = 0$.*

The conditions (i) and (ii) in Assumption 3 hold for many activation functions like Sigmoid, Tanh or smoothed ReLU functions, while (iii) can be achieved by adding an offset mapping before the activation function if there is a point x such that $g(x) = 0$.

Assumption 4 (Loss function). *The loss $\ell(\cdot, \cdot)$ is smooth with respect to the first input, i.e. $\|\nabla_1 \ell(y_1, y) - \nabla_1 \ell(y_2, y)\| \leq L_{\ell,1} \|y_1 - y_2\|, \forall y_1, y_2, y$; lower bounded, i.e. $\ell(y_1, y_2) \geq f^*, \forall y_1, y_2$.*

Aside from the assumptions, to avoid saturation during training, following the setting in [20], the saturation degree is assumed to be bounded.

Assumption 5 (Bounded Saturation). *There exists a positive constant $W_{\max} < \tau$ such that all the weight $W_k^{(m)}, m \in [M]$ is ℓ_∞ -norm bounded, i.e., $\|W_k^{(m)}\|_\infty \leq W_{\max, \infty} < \tau, \forall k \in [K]$. The ratio $W_{\max, \infty}/\tau$ is termed saturation degree.*

From the physical perspective, Assumption 5 requires that the weight can be represented by a conductance state in the dynamic range [20]. It is possible since the trainable weights always remain bounded in a small neighborhood of the initialization points during training [33–35], especially for overparameterized networks in digital training. Given $W_{\max, \infty}$ is sufficiently large to include this neighborhood, Assumption 5 holds. While it is possible to prove this assumption as in [36], we adopt it to focus on revealing key insights into the effect of pipeline training.

B. Iteration complexity of pipeline training

Next, we present the convergence rate of analog SGD with pipelines. In non-convex optimization tasks like the DNN training, it is standard to use the stationary measure as $E_K := \frac{1}{K} \sum_{k=0}^{K-1} \mathbb{E}[\|\nabla f(W_k)\|^2]$. As a warm-up, we investigate the convergence of the synchronous pipeline, Analog-SGD-SP.

Theorem 1 (Iteration complexity, Analog-SGD-SP). *Under Assumption 1–5, if the learning rate is set as $\alpha = \sqrt{\frac{B(f(W_0) - f^*)}{\sigma^2 L_f K}}$ and K is sufficiently large such that $\alpha \leq \frac{1}{L}$, it holds that*

$$E_K \leq 4 \sqrt{\frac{(f(W_0) - f^*) \sigma^2 L_f}{BK}} \frac{1}{1 - W_{\max, \infty}^2 / \tau^2} + \sigma^2 S$$

where B is the number of micro-batches, and the constant S is given by $S := \frac{W_{\max, \infty} / \tau^2}{1 - W_{\max, \infty} / \tau^2}$.

The proof of Theorem 1 is deferred to Appendix D. Analog-SGD-SP converges in the rate $\mathcal{O}(\sqrt{\sigma^2 / (BK)})$, which matches the rate of digital SGD [37]. Besides, the asymmetric bias introduces an additional term $\sigma^2 S$, which is independent of K and hence referred to as *asymptotic*

error, which also occurs in Analog-SGD-WOP [20], and can be mitigated by a well-designed AIMC accelerator or error-correction algorithms [19, 20, 22]. Next, we provide the iteration complexity of Analog-SGD-AP.

Theorem 2 (Iteration complexity, Analog-SGD-AP). *Under Assumption 1–5, if the learning rate is set as $\alpha = \sqrt{\frac{f(W_0) - f^*}{\sigma^2 L_f K}}$ and K is sufficiently large such that $\alpha \leq \frac{1}{L_f}$, it holds that*

$$E_K \leq 4\sqrt{\frac{(f(W_0) - f^*)\sigma^2 L_f}{K}} \frac{1}{1 - (1+u)W_{\max, \infty}^2/\tau^2} + \sigma^2 S' + \mathcal{O}\left(\frac{1+1/u}{K}\right) \quad (12)$$

where $u > 0$ is any number and S' denotes the amplification factor given by $S' := \frac{(1+u)W_{\max}^2/\tau^2}{1 - (1+u)W_{\max}^2/\tau^2}$.

The proof of Theorem 2 is deferred to Appendix E. Similar to Analog-SGD-WOP or Analog-SGD-SP, we have *asymptotic error* $\sigma^2 S'$, which vanishes for a well-designed AIMC accelerator or can be mitigated by error-correction algorithms [19, 20]. Moreover, since $\mathcal{O}\left(\frac{1+1/u}{K}\right)$ is not the dominant term, one can set a small u so that Analog-SGD-AP achieves the same convergence rate as the Analog-SGD-WOP [20].

Remark 1. *As a side product, we also provide an enhanced convergence analysis for SGD with asynchronous pipeline training on digital accelerators, detailed in Theorem 3 in the Appendix F. Our analysis, based on a novel Lyapunov function, shows that asynchronous pipeline effects appear only in higher-order terms, which does not slow down digital SGD, and the analysis is tighter than [32].*

C. Proof sketch of Theorem 2

In this subsection, we highlight the key steps of the proof towards Theorem 2.

(Step I) Smoothness of the objective. Before analyzing the training dynamic, we show that the objective is smooth. Recall that $\nabla_{W^{(m)}} f(W; \xi) = \delta^{(m)} \otimes x^{(m)}$, we first show that under the assumptions of DNN structures, both $\delta^{(m)}$ and $x^{(m)}$ are smooth. Using slightly abusing notations, we denote the forward and backward signals computed by W as $x^{(m)}$ and $\delta^{(m)}$, respectively; and denote the ones computed by \tilde{W} as $\tilde{x}^{(m)}$ and $\tilde{\delta}^{(m)}$, respectively. The following lemma show that for each layer m , if we regard the signals as functions of weights, they are smooth functions.

Lemma 1 (Signal stability). *Denote the forward signals computed by W and \tilde{W} as $x^{(m)}$ and $\tilde{x}^{(m)}$, respectively, and denote the backward signals as $\delta^{(m)}$ and $\tilde{\delta}^{(m)}$, respectively.*

$$\|\tilde{x}^{(m)} - x^{(m)}\|^2 \leq C_{x'}^{(m)} \|\tilde{W} - W\|^2, \quad (13)$$

$$\|\tilde{z}^{(m)} - z^{(m)}\|^2 \leq C_{z'}^{(m)} \|\tilde{W} - W\|^2, \quad (14)$$

$$\|\tilde{\delta}^{(m)} - \delta^{(m)}\|^2 \leq C_{\delta'}^{(m)} \|\tilde{W} - W\|^2, \quad (15)$$

where $C_{x'}^{(m)}$, $C_{z'}^{(m)}$, and $C_{\delta'}^{(m)}$ are constants that depend on the DNN architecture.

Based on this lemma, we prove the objective $f(W; \xi)$ is smooth.

Lemma 2 (Smoothness of the objective). *Under Assumption 2–5, the objective is L_f -smooth with respect to W , i.e. $\forall \xi = (x, y)$, $\|\nabla f(W; \xi) - \nabla f(\tilde{W}; \xi)\| \leq L_f \|W - \tilde{W}\|$, where L_f is a constant depending on the DNN architecture.*

Lemma 2 enables us to adapt the tools from [37] to obtain the sufficient descent of the function value. However, the bias from the asymmetric update and stale signals from the asynchronous pipelining accumulates layer by layer within the DNN and eventually lead to an extra term in the upper bound. Next step we quantify the error of the stale signals.

(Step II) Error of stale signals. Similar to Step I, we begin from analyzing the error of $x^{(m)}$ and $\delta^{(m)}$. However, the stale signal involves the weights at different iterations and introduces additional errors. Intuitively, the error of forward signal $\tilde{x}_k^{(m)}$ comes from the stale weight $W_{k-(M-m)}^{(m)}$ as shown by (8); while the error of the backward signal arises from the error of the forward signal. It motivated us to bound the error by the delay. Since the error between latest $W_k^{(m')}$ and the stale weight $W_{k-(M-m)}^{(m')}$ can be decomposed as

$$W_k^{(m')} - W_{k-(M-m)}^{(m')} = \sum_{k'=k-(M-m')}^{k-1} (W_{k'+1}^{(m')} - W_{k'}^{(m')}), \quad (16)$$

the following accumulated delay of layer m can be used for analyzing the upper bound of the

stale signals' error

$$\psi_k := \sum_{m'=1}^M \sum_{k'=k-(M-m')}^{k-1} \|\Delta_{k'}^{(m')}\|^2 \quad (17)$$

where $\Delta_k^{(m)} := W_{k+1}^{(m)} - W_k^{(m)}$ is the difference between consecutive weights at iteration k .

Lemma 3 (Delay error of signals). *Under Assumption 2–4, the difference between the latest and stale signals generated by Analog-SGD-AP are bounded, i.e., $\forall m \in [M + 1]$*

$$\|\tilde{x}_k^{(m)} - x_k^{(m)}\| \leq C_x^{(m)} \psi_k, \quad (18)$$

$$\|\tilde{z}_k^{(m)} - z_k^{(m)}\| \leq C_z^{(m)} \psi_k, \quad (19)$$

$$\|\tilde{\delta}_k^{(m)} - \delta_k^{(m)}\| \leq C_\delta^{(m)} \psi_k, \quad (20)$$

where $C_x^{(m)}$, $C_z^{(m)}$, and $C_\delta^{(m)}$ are constants that depends on the DNN architecture.

Remark 2. *The inequalities in Lemma 1 and 3 have a similar form, but they provide upper bounds for different error: in Lemma 1, two signals are computed on two arbitrary weights W and \tilde{W} , while in Lemma 3, two signals are generated by Analog-SGD-AP.*

(Step III) Sufficient descent of the objective. Building on the results in Steps I and II, we will analyze the sufficient descent of the objective function. However, due to the asymmetric bias of the AIMC accelerators, the convergence results for analog SGD are still non-trivial.

Lemma 4 (Sufficient descent). *Under Assumption 1–5, the objective function $f(W_k)$ satisfies*

$$\begin{aligned} \mathbb{E}_{\xi_k} [f(W_{k+1})] - f(W_k) &\lesssim -\frac{\alpha}{2} \left(1 - (1+u) \frac{\|W_k\|_\infty^2}{\tau^2} \right) \|\nabla f(W_k)\|^2 + \alpha^2 L_f \sigma^2 \\ &\quad + \frac{\alpha \sigma^2}{2\tau^2} (1+u) \|W_k\|_\infty^2 - \frac{1}{4\alpha} \mathcal{O}(\mathbb{E}_{\xi_k} [\|W_{k+1} - W_k\|^2]) + C_\psi \mathbb{E}_{\xi_k} [\psi_k] \end{aligned} \quad (21)$$

where \lesssim performs non-essential approximation on the upper bound of descent.

From Lemma 4, we notice that the accumulated delays ψ_k appear in the descent lemma, but intuitively they vanish when the algorithm converges according to its definition.

(Step IV) Construction of the Lyapunov function. To compensate for this term in equation

(21), we design the following Lyapunov function.

$$\mathbb{V}_k := f(W_k) - f^* + C_\psi \Psi_k \quad (22)$$

where the auxiliary function Ψ_k is defined as

$$\Psi_k := \sum_{m'=1}^M \sum_{k'=k-(M-m')}^{k-1} (k' - k + M) \|\Delta_{k'}^{(m')}\|^2 \quad (23)$$

and C_ψ is a constant. To achieve the dynamics of Ψ_k , we derive that

$$\begin{aligned} \Psi_{k+1} &= \sum_{m'=1}^M \sum_{k'=k+1-(M-m')}^k (k' - (k+1) + M) \|\Delta_{k'}^{(m')}\|^2 \\ &= \sum_{m'=1}^M \sum_{k'=k+1-(M-m')}^k (k' - k + M) \|\Delta_{k'}^{(m')}\|^2 - \sum_{m'=1}^M \sum_{k'=k+1-(M-m')}^k \|\Delta_{k'}^{(m')}\|^2 \end{aligned} \quad (24)$$

Let the index of the inner summation of the first term in the RHS of (24) begin from $k - (M - m')$ instead of $k + 1 - (M - m')$, we have

$$\begin{aligned} &\sum_{m'=1}^M \sum_{k'=k+1-(M-m')}^{k-1} (k' - k + M) \|\Delta_{k'}^{(m')}\|^2 \\ &= \sum_{m'=1}^M \sum_{k'=k-(M-m')}^{k-1} (k' - k + M) \|\Delta_{k'}^{(m')}\|^2 + M \sum_{m'=1}^M \|\Delta_k^{(m')}\|^2 - \sum_{m'=1}^M m' \|\Delta_{k-(M-m')}^{(m')}\|^2 \\ &= \Psi_k + M \|W_{k+1} - W_k\|^2 - \sum_{m'=1}^M m' \|\Delta_{k-(M-m')}^{(m')}\|^2 \end{aligned} \quad (25)$$

where the last equality holds by definition of $\Delta_k^{(m')}$, i.e.,

$$\sum_{m'=1}^M \|\Delta_k^{(m')}\|^2 = \sum_{m'=1}^M \|W_{k+1}^{(m')} - W_k^{(m')}\|^2 = \|W_{k+1} - W_k\|^2. \quad (26)$$

Plugging (25) into (24) yields $\Psi_{k+1} \leq \Psi_k - \psi_k + M \|W_{k+1} - W_k\|^2$, which gives a negative ψ_k .

We then show that the Lyapunov functions have sufficient descent if C_ψ is properly chosen, i.e.,

$$\mathbb{E}_{\xi_k}[\mathbb{V}_{k+1}] - \mathbb{V}_k \lesssim -\frac{\alpha}{2} \left(1 - (1+u) \frac{\|W_k\|_\infty^2}{\tau^2} \right) \|\nabla f(W_k)\|^2 + \alpha^2 L_f \sigma^2 + \frac{\alpha \sigma^2}{2\tau^2} (1+u) \|W_k\|_\infty^2. \quad (27)$$

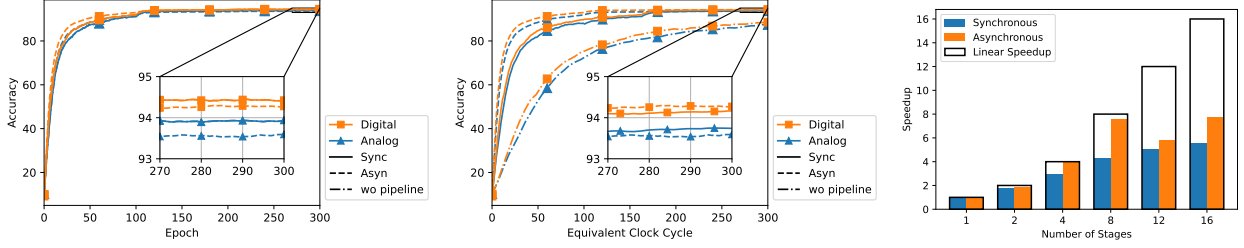


Fig. 4: Training ResNet models on CIFAR10 dataset via vanilla model parallelism without pipeline (wo pipeline), synchronous pipeline (Sync), and asynchronous pipeline (Asyn). **(Left)** Accuracy-vs-Epoch reflects sample complexity. **(Middle)** Accuracy-vs-Clock cycle. **(Right)** Speedup of the proposed pipeline training methods on AIMC accelerators as the number of stages increases compared with the single machine training case (stage=1). We ignore the communication latency since the asynchronous pipeline does not introduce obvious extra latency.

Reorganizing the inequality above yields Theorem 2.

D. Sampling and wall-clock complexity

Sample complexity measures the computational cost required to achieve the desired accuracy, whereas in model parallelism, the computation of different stages overlaps. Therefore, we are also interested in the wall-clock time it takes. In this section, we first study the sample complexity, defined as the minimum number of gradient computations required to achieve the desired error ϵ . Due to asymptotic error, we define the *sample complexity* in analog training as the minimum micro-batch needed for achieving $E_K \leq \epsilon + E$, where E is the asymptotic error, i.e. $\sigma^2 S$ for Analog-SGD-WOP/Analog-SGD-SP and $\sigma^2 S'$ for Analog-SGD-AP, respectively. Noticing that the former requires B micro-batches at each iteration while the latter requires 1, we have the following conclusion.

Corollary 1 (Sample complexity). *The sample complexities of Analog-SGD-WOP or Analog-SGD-SP are $\mathcal{O}(\sigma^2 \epsilon^{-2})$, while that of the Analog-SGD-AP is $\mathcal{O}(\sigma^2 \epsilon^{-2} + \epsilon^{-1})$.*

This shows that three model parallelisms share the same dominant term $\mathcal{O}(\sigma^2 \epsilon^{-2})$ in the sample complexity, while Analog-SGD-AP shows down by a non-dominant term $\mathcal{O}(\epsilon^{-1})$. Since the computing is overlapped, the computation density is also needed to yield the number of clock cycles needed to achieve the ϵ accuracy.

Computation density. In an ideal scenario, a micro-batch requires $2M$ clock cycles for forward and backward passes, distributed equally across M accelerators, taking 2 clock cycles per micro-batch. *Computation density* measures how closely an algorithm approaches this ideal. Let $N_c(t)$ be the number of micro-batches processed in t clock cycles. We define computation density as the limit ratio of ideal processing time to real time: $\lim_{t \rightarrow \infty} \frac{2N_c(t)}{t}$, where the factor 2 indicates that micro-batch processing involves forward and backward passes. Analog-SGD-WOP takes $2M$ cycles per micro-batch, yielding computation density $1/M$. In Analog-SGD-SP, it takes $2(M+B-1)$ clock cycles to process B micro-batches, resulting in a density of $B/(M+B-1)$. Analog-SGD-AP achieves a density of 1, as all accelerators remain active during training. Similar to sample complexity, *wall-clock complexity* is defined as the minimum clock cycle needed for achieving $E_K \leq \varepsilon + E$, where E is the asymptotic error. Wall-clock complexity is achieved by dividing the sample complexity by the computation density. The following corollary summarizes the clock cycle complexity of different pipeline strategies.

Corollary 2 (Wall-clock complexity). *The wall-clock complexities of Analog-SGD-WOP, Analog-SGD-SP, and Analog-SGD-AP are $\mathcal{O}(M\sigma^2\varepsilon^{-2})$, $\mathcal{O}((M+B-1)B^{-1}\sigma^2\varepsilon^{-2})$, and $\mathcal{O}(\sigma^2\varepsilon^{-2} + \varepsilon^{-1})$, respectively.*

Takeaway. Analog-SGD-AP maximizes the computation density of DNN training only at the cost of a higher-order error term compared with the synchronous pipeline.

IV. NUMERICAL SIMULATIONS

In this section, we aim to numerically verify the theoretical benefits of Analog-SGD-AP. We test the analog methods in an open-source IBM Analog Hardware Acceleration Kit (AIHWKIT) [38]; see github.com/IBM/aihwkit. The pipeline parallelism is also simulated on a single GPU. To get the *equivalent clock cycle* in the figures, we map the epoch to clock cycle by dividing the computation density.

Simulation settings. In the simulations, we train ResNet models on two benchmark datasets: CIFAR10 and CIFAR100. The CIFAR10 dataset consists of 60,000 32×32 color images across

		CIFAR10		
		speedup	accuracy (mid)	accuracy (end)
Digital	w.o. pipeline	1.00	88.63 \pm 0.70	94.32 \pm 0.12
	synchronous	3.69	94.17 \pm 0.15	94.32 \pm 0.12
	asynchronous	6.18	94.25 \pm 0.17	94.25 \pm 0.16
Analog	w.o. pipeline	1.00	88.04 \pm 0.58	93.95 \pm 0.07
	synchronous	3.69	93.75 \pm 0.08	93.95 \pm 0.07
	asynchronous	5.66	93.60 \pm 0.05	93.60 \pm 0.07

		CIFAR100		
		speedup	accuracy (mid)	accuracy (end)
Digital	w.o. pipeline	1.00	67.85 \pm 0.52	73.99 \pm 0.19
	synchronous	3.69	73.91 \pm 0.19	73.99 \pm 0.19
	asynchronous	8.19	74.64 \pm 0.48	74.64 \pm 0.53
Analog	w.o. pipeline	1.00	61.35 \pm 0.73	72.29 \pm 0.30
	synchronous	3.69	72.14 \pm 0.31	72.29 \pm 0.30
	asynchronous	6.17	72.69 \pm 0.30	72.64 \pm 0.21

TABLE II: Training ResNet10 on CIFAR10/CIFAR100 dataset via vanilla model parallelism without pipeline (wo pipeline), synchronous pipeline (Sync), and asynchronous pipeline (Asyn). The speedup is computed by comparing the number of clock cycles required to achieve 93% accuracy. The test accuracy and standard deviation at clock cycle 300 (mid) and epoch 300 (end) are reported.

B_{micro}	Synchronous			Asynchronous			
	speedup	acc (mid)	acc (end)	speedup	acc (mid)	acc (end)	
D	16	3.69		6.18	94.25 \pm 0.17	94.25 \pm 0.16	
	32	2.67		6.06	94.27 \pm 0.18	94.28 \pm 0.20	
	64	1.71	94.17 \pm 0.15	94.32 \pm 0.12	6.00	94.09 \pm 0.13	94.08 \pm 0.15
	128	1.00			5.83	93.68 \pm 0.39	93.67 \pm 0.38
A	16	3.69	93.75 \pm 0.08	93.95 \pm 0.07	5.66	93.60 \pm 0.05	93.60 \pm 0.07
	32	2.67	93.57 \pm 0.12	93.95 \pm 0.07	5.88	93.62 \pm 0.13	93.61 \pm 0.11
	64	1.71	90.86 \pm 0.44	93.95 \pm 0.07	5.88	93.58 \pm 0.14	93.60 \pm 0.17
	128	1.00	88.04 \pm 0.58	93.95 \pm 0.07	4.89	93.36 \pm 0.06	93.37 \pm 0.06

TABLE III: Training Resnet10 model on CIFAR10 dataset under different micro-batch size setting. Test accuracy and standard deviation at clock cycle 300 (mid) and epoch 300 (end) are reported. The speedup is computed by comparing the number of clock cycles required to achieve 93% target accuracy. The accuracy of synchronous is not affected by micro-batch size.

10 classes, with each class representing a distinct category such as airplanes, cars, and birds. The CIFAR100 dataset is similar in format but includes 100 classes. Each model was trained over 300 epochs using a mini-batch size of $B_{\text{mini}} = 128$ and micro-batch-size $B_{\text{micro}} = 16$ by default. The initial learning rate of $\alpha = 0.1$ was employed, while for Resnet34 with stage numbers $M = 12, 16$, the initial learning rate is $\alpha = 0.01$. The transfer learning rate of Tiki-Taka

is chosen to be equal to the initial learning rate and kept fit during the training. The learning rate α was reduced by a factor of 10 every 100 epochs. To further enhance the model’s ability to generalize across diverse images, we applied data augmentation techniques such as random cropping, horizontal flipping, and color jittering [39]. The other setting follows the default settings of AIHWKIT, including output noise (0.5 % of the quantization bin width), quantization and clipping (output range set to 20, output noise 0.1, and input and output quantization to 8 bits). Noise and bound management techniques are used in [40]. A learnable scaling factor is set after each analog layer, which is updated using digital SGD.

Sample complexity and wall-clock complexity. We train a ResNet10 for an image classification task on CIFAR10. We map the first 5 stages on digital accelerators while the last one onto an AIMC (analog) accelerator. The results on the left of Fig. 4 show that the accuracy-epoch curves of all three pipeline strategies on AIMC accelerators almost overlap and even match the performance of digital SGD, implying all of these algorithms have the same sample complexity and align with Theorem 1–2 and Corollary 1. Moreover, as indicated by Corollary 2, the walk-clock complexity of the Analog-SGD-AP pipeline is the lowest owing to the highest computation density. The results on the CIFAR100 training are reported in Table II, whose conclusion is the same as above.

Effect of stage/accelerator number. We also explored the impact of increasing the number of accelerators on the speedup achieved through pipeline parallelism; see Figure 4, Right. In the simulations, we train a ResNet34 model [41] on the CIFAR10 dataset. The model is separated into $M = 1, 2, 4, 8, 12, 16$ stages. Assuming the model can be evenly divided into multiple stages, and the equivalent clock cycle needed to compute the entire model is fixed. The results reveal that the asynchronous pipeline achieves linear speedup at least within the range of 1 – 8 accelerators.

Effect of micro-batch size. We also report the effect of micro-batch sizes in Table III. We fit the mini-batch size as $B_{\text{mini}} = 128$ and change the micro-batch size. For synchronous pipeline training, increasing the batch size improves the speedup on both digital and analog accelerators. Moreover, asynchronous pipeline training consistently results in higher speedup compared to the synchronous version. The trade-off is that the asynchronous pipeline sacrifices accuracy and can

only reach lower accuracy when the training time is sufficiently long.

V. CONCLUSIONS AND LIMITATIONS

This paper theoretically investigates the pipeline algorithms for AIMC accelerators with respect to convergence and computation complexity. To unlock the full potential of pipeline training, asynchronous pipeline discards the synchronization at the end of one mini-batch to maximize the accelerator usage. We theoretically demonstrate that `Analog-SGD-AP` achieves maximal computational density with only a slight sacrifice in sample complexity through higher-order terms, which brings extraordinary speedup on wall-clock complexity. Simulations validate our theoretical findings. A limitation of this work is the lack of real hardware validation, but this is a necessary step for every new technology and is widely used in current research regarding the algorithm development for AIMC accelerators. Future work should verify its efficiency as the technology becomes mature.

REFERENCES

- [1] Hugo Touvron, Louis Martin, Kevin Stone, Peter Albert, Amjad Almahairi, Yasmine Babaei, Nikolay Bashlykov, Soumya Batra, Prajwal Bhargava, Shruti Bhosale, et al. Llama 2: Open foundation and fine-tuned chat models. *arXiv preprint arXiv:2307.09288*, 2023.
- [2] Shubham Jain et al. Neural network accelerator design with resistive crossbars: Opportunities and challenges. *IBM Journal of Research and Development*, 63(6):10–1, 2019.
- [3] Shen Li, Yanli Zhao, Rohan Varma, Omkar Salpekar, Pieter Noordhuis, Teng Li, Adam Paszke, Jeff Smith, Brian Vaughan, Pritam Damania, et al. Pytorch distributed: Experiences on accelerating data parallel training. *arXiv preprint arXiv:2006.15704*, 2020.
- [4] Priya Goyal, Piotr Dollár, Ross Girshick, Pieter Noordhuis, Lukasz Wesolowski, Aapo Kyrola, Andrew Tulloch, Yangqing Jia, and Kaiming He. Accurate, large minibatch SGD: Training Imagenet in 1 hour. *arXiv preprint arXiv:1706.02677*, 2017.
- [5] Yang You, Jing Li, Sashank Reddi, Jonathan Hseu, Sanjiv Kumar, Srinadh Bhojanapalli, Xiaodan Song, James Demmel, Kurt Keutzer, and Cho-Jui Hsieh. Large batch optimization

- for deep learning: Training BERT in 76 minutes. In *International Conference on Learning Representations*, 2020.
- [6] Weizheng Xu, Youtao Zhang, and Xulong Tang. Parallelizing DNN training on GPUs: Challenges and opportunities. In *Companion Proceedings of the Web Conference*, pages 174–178, 2021.
- [7] Yanping Huang, Youlong Cheng, Ankur Bapna, Orhan Firat, Dehao Chen, Mia Chen, HyoukJoong Lee, Jiquan Ngiam, Quoc V Le, Yonghui Wu, et al. Gpipe: Efficient training of giant neural networks using pipeline parallelism. *Advances in neural information processing systems*, 32, 2019.
- [8] Chiheon Kim, Heungsub Lee, Myungryong Jeong, Woonhyuk Baek, Boogeon Yoon, Ildoo Kim, Sungbin Lim, and Sungwoong Kim. torchgpipe: On-the-fly pipeline parallelism for training giant models. *arXiv preprint arXiv:2004.09910*, 2020.
- [9] Jie Ren, Samyam Rajbhandari, Reza Yazdani Aminabadi, Olatunji Ruwase, Shuangyan Yang, Minjia Zhang, Dong Li, and Yuxiong He. Zero-offload: Democratizing billion-scale model training. In *USENIX Annual Technical Conference*, pages 551–564, 2021.
- [10] Yanli Zhao, Andrew Gu, Rohan Varma, Liang Luo, Chien-Chin Huang, Min Xu, Less Wright, Hamid Shojanazeri, Myle Ott, Sam Shleifer, et al. Pytorch FSDP: experiences on scaling fully sharded data parallel. *arXiv preprint arXiv:2304.11277*, 2023.
- [11] Mohammad Shoeybi, Mostofa Patwary, Raul Puri, Patrick LeGresley, Jared Casper, and Bryan Catanzaro. Megatron-lm: Training multi-billion parameter language models using model parallelism. *arXiv preprint arXiv:1909.08053*, 2019.
- [12] Shenggui Li, Hongxin Liu, Zhengda Bian, Jiarui Fang, Haichen Huang, Yuliang Liu, Boxiang Wang, and Yang You. Colossal-AI: A unified deep learning system for large-scale parallel training. In *International Conference on Parallel Processing*, pages 766–775, 2023.
- [13] Tao Sun, Robert Hannah, and Wotao Yin. Asynchronous coordinate descent under more realistic assumptions. *Advances in Neural Information Processing Systems*, 30, 2017.
- [14] Zhouyuan Huo, Bin Gu, Heng Huang, et al. Decoupled parallel backpropagation with

- convergence guarantee. In *International Conference on Machine Learning*, pages 2098–2106. PMLR, 2018.
- [15] Tayfun Gokmen and Yurii Vlasov. Acceleration of deep neural network training with resistive cross-point devices: Design considerations. *Frontiers in neuroscience*, 10:333, 2016.
- [16] Peng Yao, Huaqiang Wu, Bin Gao, Sukru Burc Eryilmaz, Xueyao Huang, Wenqiang Zhang, Qingtian Zhang, Ning Deng, Luping Shi, H-S Philip Wong, et al. Face classification using electronic synapses. *Nature communications*, 8(1):15199, 2017.
- [17] Zhongrui Wang, Can Li, Peng Lin, Mingyi Rao, Yongyang Nie, Wenhao Song, Qinru Qiu, Yunning Li, Peng Yan, John Paul Strachan, et al. In situ training of feed-forward and recurrent convolutional memristor networks. *Nature Machine Intelligence*, 1(9):434–442, 2019.
- [18] Geoffrey W Burr, Robert M Shelby, Severin Sidler, Carmelo Di Nolfo, Junwoo Jang, Irem Boybat, Rohit S Shenoy, Pritish Narayanan, Kumar Virwani, Emanuele U Giacometti, et al. Experimental demonstration and tolerancing of a large-scale neural network (165 000 synapses) using phase-change memory as the synaptic weight element. *IEEE Transactions on Electron Devices*, 62(11):3498–3507, 2015.
- [19] Tayfun Gokmen and Wilfried Haensch. Algorithm for training neural networks on resistive device arrays. *Frontiers in Neuroscience*, 14, 2020.
- [20] Zhaoxian Wu, Tayfun Gokmen, Malte J Rasch, and Tianyi Chen. Towards exact gradient-based training on analog in-memory computing. In *Advances in Neural Information Processing Systems*, 2024.
- [21] Zhaoxian Wu, Quan Xiao, Tayfun Gokmen, Omobayode Fagbohunbe, and Tianyi Chen. Analog in-memory training on general non-ideal resistive elements: The impact of response functions. *arXiv preprint arXiv:2502.06309*, 2025.
- [22] Tayfun Gokmen. Enabling training of neural networks on noisy hardware. *Frontiers in Artificial Intelligence*, 4:1–14, 2021.
- [23] Malte J Rasch, Fabio Carta, Omobayode Fagbohunbe, and Tayfun Gokmen. Fast offset

- corrected in-memory training. *arXiv preprint arXiv:2303.04721*, 2023.
- [24] Murat Onen, Tayfun Gokmen, Teodor K Todorov, Tomasz Nowicki, Jesús A Del Alamo, John Rozen, Wilfried Haensch, and Seyoung Kim. Neural network training with asymmetric crosspoint elements. *Frontiers in artificial intelligence*, 5, 2022.
- [25] Jindan Li, Zhaoxian Wu, Gaowen Liu, Tayfun Gokmen, and Tianyi Chen. In-memory training on analog devices with limited conductance states via multi-tile residual learning. *arXiv preprint arXiv:2510.02516*, 2025.
- [26] Atli Kosson, Vitaliy Chiley, Abhinav Venigalla, Joel Hestness, and Urs Koster. Pipelined backpropagation at scale: training large models without batches. *Proceedings of Machine Learning and Systems*, 3:479–501, 2021.
- [27] Deepak Narayanan, Aaron Harlap, Amar Phanishayee, Vivek Seshadri, Nikhil R Devanur, Gregory R Ganger, Phillip B Gibbons, and Matei Zaharia. Pipedream: generalized pipeline parallelism for DNN training. In *Proceedings of the 27th ACM symposium on operating systems principles*, pages 1–15, 2019.
- [28] Yangrui Chen, Cong Xie, Meng Ma, Juncheng Gu, Yanghua Peng, Haibin Lin, Chuan Wu, and Yibo Zhu. SApipe: Staleness-aware pipeline for data parallel DNN training. *Advances in Neural Information Processing Systems*, 35:17981–17993, 2022.
- [29] Youjie Li, Mingchao Yu, Songze Li, Salman Avestimehr, Nam Sung Kim, and Alexander Schwing. Pipe-SGD: A decentralized pipelined SGD framework for distributed deep net training. *Advances in Neural Information Processing Systems*, 31, 2018.
- [30] Ali Shafiee, Anirban Nag, Naveen Muralimanohar, Rajeev Balasubramonian, John Paul Strachan, Miao Hu, R Stanley Williams, and Vivek Srikumar. ISAAC: A convolutional neural network accelerator with in-situ analog arithmetic in crossbars. *ACM SIGARCH Computer Architecture News*, 44(3):14–26, 2016.
- [31] Linghao Song, Xuehai Qian, Hai Li, and Yiran Chen. Pipelayer: A pipelined ReRAM-based accelerator for deep learning. In *IEEE international symposium on high performance computer architecture*, pages 541–552. IEEE, 2017.
- [32] An Xu, Zhouyuan Huo, and Heng Huang. On the acceleration of deep learning model par-

- allelism with staleness. In *IEEE Conference on Computer Vision and Pattern Recognition*, pages 2088–2097, 2020.
- [33] Samet Oymak and Mahdi Soltanolkotabi. Overparameterized nonlinear learning: Gradient descent takes the shortest path? In *International Conference on Machine Learning*, pages 4951–4960. PMLR, 2019.
- [34] Chaoyue Liu, Libin Zhu, and Mikhail Belkin. Loss landscapes and optimization in over-parameterized non-linear systems and neural networks. *Applied and Computational Harmonic Analysis*, 59:85–116, 2022.
- [35] Difan Zou and Quanquan Gu. An improved analysis of training over-parameterized deep neural networks. *Advances in neural information processing systems*, 32, 2019.
- [36] Jiawei Zhang, Peijun Xiao, Ruoyu Sun, and Zhiquan Luo. A single-loop smoothed gradient descent-ascent algorithm for nonconvex-concave min-max problems. *Advances in neural information processing systems*, 2020.
- [37] Léon Bottou, Frank E Curtis, and Jorge Nocedal. Optimization methods for large-scale machine learning. *SIAM review*, 60(2):223–311, 2018.
- [38] Malte J Rasch, Diego Moreda, Tayfun Gokmen, Manuel Le Gallo, Fabio Carta, Cindy Goldberg, Kaoutar El Maghraoui, Abu Sebastian, and Vijay Narayanan. A flexible and fast PyTorch toolkit for simulating training and inference on analog crossbar arrays. *IEEE International Conference on Artificial Intelligence Circuits and Systems*, pages 1–4, 2021.
- [39] Ekin D Cubuk, Barret Zoph, Dandelion Mane, Vijay Vasudevan, and Quoc V Le. Autoaugment: Learning augmentation policies from data. *arXiv preprint arXiv:1805.09501*, 2018.
- [40] Tayfun Gokmen, Murat Onen, and Wilfried Haensch. Training deep convolutional neural networks with resistive cross-point devices. *Frontiers in neuroscience*, 11:538, 2017.
- [41] Zifeng Wu, Chunhua Shen, and Anton Van Den Hengel. Wider or deeper: Revisiting the resnet model for visual recognition. *Pattern recognition*, 90:119–133, 2019.

Appendix

APPENDIX A

ANALOG SGD WITH ASYNCHRONOUS PIPELINE IN DIFFERENT PERSPECTIVE

Involving multiple accelerators and data at each time step, pipeline algorithms, especially the asynchronous pipeline, are usually hard to figure out. To facilitate the understanding, we list the Analog SGD under two different perspectives. In *accelerator perspective*, we pay more attention to how accelerator m processes a flow of data; see Algorithm 1. In *data perspective*, we focus on how a sample ξ_k flows through each accelerator; see Algorithm 2. To make the relationship clearer, the computation dependency is plotted in Fig. 3.

Algorithm 1 Analog SGD with asynchronous pipeline (accelerator Perspective)

- 1: **for** iteration $k = 0, 1, 2, \dots, K$ **do**
 - // Periphery device at the beginning
 - 2: Sample $\xi_k = (x_k, y_k)$ and Send $x_k^{(0)} = x_k$ to accelerator 1
 - // Accelerator $m = 1, 2, \dots, M$ in parallel
 - 3: Receive input $\tilde{x}_k^{(m)}$ from accelerator $m - 1$
 - 4: Compute $\tilde{z}_k^{(m)} = W_{k-(M-m)}^{(m)} \tilde{x}_k^{(m)}$
 - 5: Compute $\tilde{x}_k^{(m+1)} = g^{(m)}(\tilde{z}_k^{(m)})$ and $\nabla g^{(m)}(\tilde{z}_k^{(m)})$
 - 6: Store input $\tilde{x}_k^{(m)}$ and $\nabla g^{(m)}(\tilde{z}_k^{(m)})$
 - 7: Receive backward signal $\tilde{\delta}_{k-(M-m)}^{(m+1)}$
 - 8: $\tilde{\delta}_k^{(m)} = \tilde{\delta}_k^{(m+1)} W_k^{(m+1)} \nabla g^{(m)}(\tilde{z}_k^{(m)})$
 - 9: $W_{k+1}^{(m)} = W_k^{(m)} - \alpha \tilde{\delta}_k^{(m)} \otimes \tilde{x}_k^{(m)} - \frac{\alpha}{\tau} |\tilde{\delta}_k^{(m)} \otimes \tilde{x}_k^{(m)}| \odot W_k^{(m)}$
 - // Periphery device at the end
 - 10: Compute $\tilde{\delta}_k^{(M)} = \nabla_{\tilde{x}^{(M+1)}} \ell(\tilde{x}^{(M+1)}, y_k) \nabla g^{(M)}(\tilde{z}^{(M)})$
 - 11: Send $\tilde{\delta}_k^{(M)}$ back to accelerator M
 - 12: **end for**
-

Algorithm 2 Analog SGD with asynchronous pipeline (Data Perspective)

```

1: for iteration  $k = 0, 1, 2, \dots, K$  do
2:   Sample  $\xi_k = (x_k, y_k)$ ,  $x_k^{(0)} = x_k$ 
3:   for all accelerator  $m = 1, 2, \dots, M$  do
4:     Compute  $\tilde{z}_k^{(m)} = W_{k-(M-m)}^{(m)} \tilde{x}_k^{(m)}$ 
5:     Compute  $\tilde{x}_k^{(m+1)} = g^{(m)}(\tilde{z}_k^{(m)})$  and  $\nabla g^{(m)}(\tilde{z}_k^{(m)})$ 
6:   end for
7:   Compute  $\tilde{\delta}_k^{(M)} = \nabla_{\tilde{x}^{(M+1)}} \ell(\tilde{x}^{(M+1)}, y_k) \nabla g^{(M)}(\tilde{z}^{(M)})$ 
8:   for all layer  $m = M, M-1, \dots, 1$  do
9:      $\tilde{\delta}_k^{(m)} = \tilde{\delta}_k^{(m+1)} W_k^{(m+1)} \nabla g^{(m)}(\tilde{z}_k^{(m)})$ 
10:     $W_{k+1}^{(m)} = W_k^{(m)} - \alpha \tilde{\delta}_k^{(m)} \otimes \tilde{x}_k^{(m)} - \frac{\alpha}{\tau} |\tilde{\delta}_k^{(m)} \otimes \tilde{x}_k^{(m)}| \odot W_k^{(m)}$ 
11:   end for
12: end for

```

APPENDIX B

USEFUL LEMMAS AND THEIR PROOF

We first bound the error of the stale variables. Define $\Delta_k^{(m)} := W_{k+1}^{(m)} - W_k^{(m)}$, which is the different between consecutive weights.

Lemma 5 (Delay error of signals, restatement of Lemma 3). *Under Assumption 2–4, the difference between the latest and stale signals generated by Analog-SGD-AP are bounded, i.e., $\forall m \in [M+1]$*

$$\|\tilde{x}_k^{(m)} - x_k^{(m)}\| \leq C_x^{(m)} \sum_{m'=1}^{m-1} \sum_{k'=k-(M-m')}^{k-1} \|\Delta_{k'}^{(m')}\|, \quad (28)$$

$$\|\tilde{z}_k^{(m)} - z_k^{(m)}\| \leq C_z^{(m)} \sum_{m'=1}^m \sum_{k'=k-(M-m')}^{k-1} \|\Delta_{k'}^{(m')}\|, \quad (29)$$

$$\|\tilde{\delta}_k^{(m)} - \delta_k^{(m)}\| \leq C_\delta^{(m)} \sum_{m'=1}^M \sum_{k'=k-(M-m')}^{k-1} \|\Delta_{k'}^{(m')}\|, \quad (30)$$

where the constants above are defined by

$$C_x^{(m)} := L_{g,0} (L_{g,0} W_{\max,2})^{m-1}, \quad (31)$$

$$C_z^{(m)} := (L_{g,0} W_{\max,2})^{m-1}, \quad (32)$$

$$C_\delta^{(m)} := (L_{g,0} W_{\max,2})^{M-m+1} (L_{\ell,1} L_{g,0}^2 + L_{\ell,0} L_{g,1}) (L_{g,0} W_{\max,2})^{M-1} \quad (33)$$

$$+ (L_{g,0}W_{\max,2})^{M-1}L_{\ell,0}L_{g,1}\frac{1 - (L_{g,0}W_{\max,2})^{M-m}}{1 - L_{g,0}W_{\max,2}}.$$

Proof of Lemma 3 and Lemma 5. We first bound the delay of the forward signal $\tilde{x}_k^{(m)}$. At the first layer, there is no delay, i.e. $\tilde{x}_k^{(1)} = x_k^{(1)} = x_k$. For other layers $m > 1$

$$\begin{aligned} & \|\tilde{x}_k^{(m+1)} - x_k^{(m+1)}\| \leq L_{g,0}\|\tilde{z}_k^{(m)} - z_k^{(m)}\| \\ &= L_{g,0}\|W_{k-(M-m)}^{(m)}\tilde{x}_k^{(m)} - W_k^{(m)}x_k^{(m)}\| \\ &= L_{g,0}\|(W_{k-(M-m)}^{(m)} - W_k^{(m)})\tilde{x}_k^{(m)} + W_k^{(m)}(\tilde{x}_k^{(m)} - x_k^{(m)})\| \\ &\stackrel{(a)}{\leq} L_{g,0}(\|W_{k-(M-m)}^{(m)} - W_k^{(m)}\|_2\|\tilde{x}_k^{(m)}\| + \|W_k^{(m)}\|_2\|\tilde{x}_k^{(m)} - x_k^{(m)}\|) \\ &\leq L_{g,0}((L_{g,0}W_{\max,2})^m\|W_{k-(M-m)}^{(m)} - W_k^{(m)}\| + W_{\max,2}\|\tilde{x}_k^{(m)} - x_k^{(m)}\|) \end{aligned} \quad (34)$$

where (a) follows the triangle inequality and the consistency of ℓ_2 -matrix norm, i.e. $\|Wu\| \leq \|W\|_2\|u\|$ where W and u are arbitrary matrices and vectors, respectively. Using triangle inequality over the first term of RHS in (34), we have

$$\|W_{k-(M-m)}^{(m)} - W_k^{(m)}\| \leq \sum_{k'=k-(M-m)}^{k-1} \|W_{k'+1}^{(m)} - W_{k'}^{(m)}\| = \sum_{k'=k-(M-m)}^{k-1} \|\Delta_{k'}^{(m)}\| \quad (35)$$

and consequently,

$$\|\tilde{x}_k^{(m+1)} - x_k^{(m+1)}\| \leq L_{g,0}(L_{g,0}W_{\max,2})^m \sum_{k'=k-(M-m)}^{k-1} \|\Delta_{k'}^{(m)}\| + L_{g,0}W_{\max,2}\|\tilde{x}_k^{(m)} - x_k^{(m)}\|. \quad (36)$$

Expanding inequality (36) from m to 1 and using the fact $\tilde{x}_k^{(1)} = x_k^{(1)} = x_k$ yield

$$\begin{aligned} & \|\tilde{x}_k^{(m)} - x_k^{(m)}\| \\ &\leq L_{g,0}(L_{g,0}W_{\max,2})^{m-1} \sum_{k'=k-(M-m+1)}^{k-1} \|\Delta_{k'}^{(m-1)}\| + L_{g,0}W_{\max,2}\|\tilde{x}_k^{(m-1)} - x_k^{(m-1)}\| \\ &\leq L_{g,0} \sum_{m'=2}^m (L_{g,0}W_{\max,2})^{m'-1} (L_{g,0}W_{\max,2})^{m-m'} \sum_{k'=k-(M-m'+1)}^{k-1} \|\Delta_{k'}^{(m'-1)}\| \\ &\leq L_{g,0}(L_{g,0}W_{\max,2})^{m-1} \sum_{m'=2}^m \sum_{k'=k-(M-m'+1)}^{k-1} \|\Delta_{k'}^{(m'-1)}\|. \end{aligned} \quad (37)$$

$$= L_{g,0}(L_{g,0}W_{\max,2})^{m-1} \sum_{m'=1}^{m-1} \sum_{k'=k-(M-m')}^{k-1} \|\Delta_{k'}^{(m')}\|.$$

where the last inequality reindexes m' in the first summation.

Noticing that (34)-(37) also implies that

$$\|z_k^{(m)} - \tilde{z}_k^{(m)}\| \leq (L_{g,0}W_{\max,2})^{m-1} \sum_{m'=1}^{m-1} \sum_{k'=k-(M-m')}^{k-1} \|\Delta_{k'}^{(m')}\|. \quad (38)$$

We then bound the delay of the backward signal $\tilde{\delta}_k^{(m)}$ for $m \in [M-1]$

$$\begin{aligned} \|\tilde{\delta}_k^{(m)} - \delta_k^{(m)}\| &= \|\delta_k^{(m+1)}W_k^{(m+1)}\nabla g^{(m)}(z_k^{(m)}) - \tilde{\delta}_k^{(m+1)}W_k^{(m+1)}\nabla g^{(m)}(\tilde{z}_k^{(m)})\| \\ &\leq \|\delta_k^{(m+1)} - \tilde{\delta}_k^{(m+1)}\| \|W_k^{(m+1)}\| \|\nabla g^{(m)}(z_k^{(m)})\| \\ &\quad + \|\tilde{\delta}_k^{(m+1)}\| \|W_k^{(m+1)}\| \|\nabla g^{(m)}(z_k^{(m)}) - \nabla g^{(m)}(\tilde{z}_k^{(m)})\| \\ &\leq L_{g,0}W_{\max,2} \|\delta_k^{(m+1)} - \tilde{\delta}_k^{(m+1)}\| + W_{\max,2}(L_{g,0}W_{\max,2})^{M-m-1} L_{\ell,0}L_{g,0}L_{g,1} \|z_k^{(m)} - \tilde{z}_k^{(m)}\| \end{aligned} \quad (39)$$

where the last inequality comes from Assumption 3 (1)-(2) and Lemma 8. Substituting (38) into (39), we can further bound (39) by

$$\begin{aligned} \|\tilde{\delta}_k^{(m)} - \delta_k^{(m)}\| &\leq L_{g,0}W_{\max,2} \|\delta_k^{(m+1)} - \tilde{\delta}_k^{(m+1)}\| \\ &\quad + W_{\max,2}(L_{g,0}W_{\max,2})^{M-m-1} L_{\ell,0}L_{g,0}L_{g,1} (L_{g,0}W_{\max,2})^{m-1} \sum_{m'=1}^{m-1} \sum_{k'=k-(M-m')}^{k-1} \|\Delta_{k'}^{(m')}\| \\ &= L_{g,0}W_{\max,2} \|\delta_k^{(m+1)} - \tilde{\delta}_k^{(m+1)}\| + (L_{g,0}W_{\max,2})^{M-1} L_{\ell,0}L_{g,1} \sum_{m'=1}^{m-1} \sum_{k'=k-(M-m')}^{k-1} \|\Delta_{k'}^{(m')}\| \\ &\leq (L_{g,0}W_{\max,2})^{M-m} \|\delta_k^{(M)} - \tilde{\delta}_k^{(M)}\| + (L_{g,0}W_{\max,2})^{M-1} L_{\ell,0}L_{g,1} \times \\ &\quad \sum_{m''=m}^{M-1} (L_{g,0}W_{\max,2})^{M-1-m''} \sum_{m'=1}^{m''-1} \sum_{k'=k-(M-m')}^{k-1} \|\Delta_{k'}^{(m')}\|. \end{aligned} \quad (40)$$

To bound the first term in the RHS of (40), we manipulate the different $\|\delta_k^{(M)} - \tilde{\delta}_k^{(M)}\|$ by

$$\|\delta_k^{(M)} - \tilde{\delta}_k^{(M)}\| \quad (41)$$

$$\begin{aligned}
&= \|\nabla_{x^{(M+1)}}\ell(x_k^{(M+1)}, y_k)\nabla g^{(M)}(z_k^{(M)}) - \nabla_{x^{(M+1)}}\ell(\tilde{x}_k^{(M+1)}, y_k)\nabla g^{(M)}(\tilde{z}_k^{(M)})\| \\
&\leq \|\nabla_{x^{(M+1)}}\ell(x_k^{(M+1)}, y_k) - \nabla_{x^{(M+1)}}\ell(\tilde{x}_k^{(M+1)}, y_k)\| \|\nabla g^{(M)}(z_k^{(M)})\| \\
&\quad + \|\nabla_{x^{(M+1)}}\ell(\tilde{x}_k^{(M+1)}, y_k)\| \|\nabla g^{(M)}(\tilde{z}_k^{(M)}) - \nabla g^{(M)}(z_k^{(M)})\| \\
&\stackrel{(a)}{\leq} L_{\ell,1}L_{g,0}\|x_k^{(M+1)} - \tilde{x}_k^{(M+1)}\| + L_{\ell,0}L_{g,1}\|\tilde{z}_k^{(M)} - z_k^{(M)}\| \\
&\leq (L_{\ell,1}L_{g,0}^2 + L_{\ell,0}L_{g,1})\|\tilde{z}_k^{(M)} - z_k^{(M)}\| \\
&\leq (L_{\ell,1}L_{g,0}^2 + L_{\ell,0}L_{g,1})(L_{g,0}W_{\max,2})^{M-1} \sum_{m'=1}^M \sum_{k'=k-(M-m')}^{k-1} \|\Delta_{k'}^{(m')}\|.
\end{aligned}$$

where (a) comes from Assumption 3 and Assumption 4.

To bound the second term in the RHS of (40), we change the upper bound of the second summation from m'' to M and get

$$\begin{aligned}
&\sum_{m''=m}^{M-1} (L_{g,0}W_{\max,2})^{M-1-m''} \sum_{m'=1}^{m''-1} \sum_{k'=k-(M-m')}^{k-1} \|\Delta_{k'}^{(m')}\| \\
&\leq \sum_{m''=m}^{M-1} (L_{g,0}W_{\max,2})^{M-1-m''} \sum_{m'=1}^M \sum_{k'=k-(M-m')}^{k-1} \|\Delta_{k'}^{(m')}\| \\
&= \frac{1 - (L_{g,0}W_{\max,2})^{M-m}}{1 - L_{g,0}W_{\max,2}} \sum_{m'=1}^M \sum_{k'=k-(M-m')}^{k-1} \|\Delta_{k'}^{(m')}\|.
\end{aligned} \tag{42}$$

Substituting (41) and (42) back into (40) we have

$$\|\tilde{\delta}_k^{(m)} - \delta_k^{(m)}\| \leq C_\delta^{(m)} \sum_{m'=1}^M \sum_{k'=k-(M-m')}^{k-1} \|\Delta_{k'}^{(m')}\| \tag{43}$$

where the constant $C_\delta^{(m)}$ is defined by

$$\begin{aligned}
C_\delta^{(m)} &:= (L_{g,0}W_{\max,2})^{M-m+1} (L_{\ell,1}L_{g,0}^2 + L_{\ell,0}L_{g,1})(L_{g,0}W_{\max,2})^{M-1} \\
&\quad + (L_{g,0}W_{\max,2})^{M-1} L_{\ell,0}L_{g,1} \frac{1 - (L_{g,0}W_{\max,2})^{M-m}}{1 - L_{g,0}W_{\max,2}}.
\end{aligned} \tag{44}$$

This completes the proof. \square

Lemma 6 (Delayed error of gradient). *Denote the stale gradient as*

$$\tilde{\nabla}_{W^{(m)}}^k f := \tilde{\delta}_k^{(m)} \otimes \tilde{x}_k^{(m)}. \quad (45)$$

The gradient delay is bounded by

$$\|\tilde{\nabla}_{W^{(m)}}^k f - \nabla_{W^{(m)}} f(W_k; \xi_k)\| \leq C_f^{(m)} \sum_{m'=1}^M \sum_{k'=k-(M-m')}^{k-1} \|\Delta_{k'}^{(m'-1)}\|. \quad (46)$$

where the constant $C_f^{(m)}$ is defined by

$$C_f^{(m)} := (L_{g,0} W_{\max,2})^m C_\delta^{(m)} + (L_{g,0} W_{\max,2})^{M-m} L_{\ell,0} L_{g,0} C_x^{(m)}. \quad (47)$$

Consequently, the norm square of the gradient delay is bounded by

$$\|\tilde{\nabla}^k f - \nabla f(W_k; \xi_k)\|^2 \leq C_f^2 \sum_{m'=1}^M \sum_{k'=k-(M-m')}^{k-1} \|\Delta_{k'}^{(m')}\|^2 \quad (48)$$

where the constant C_f is defined by

$$C_f := M \sqrt{\sum_{m=1}^M (C_f^{(m)})^2}. \quad (49)$$

Proof of Lemma 6. By definition, the delay error is bounded by

$$\begin{aligned} & \|\tilde{\nabla}_{W^{(m)}}^k f - \nabla_{W^{(m)}} f(W_k; \xi_k)\| \|\tilde{\delta}_k^{(m)} \otimes \tilde{x}_k^{(m)} - \delta_k^{(m)} \otimes x_k^{(m)}\| \\ &= \|(\tilde{\delta}_k^{(m)} - \delta_k^{(m)}) \otimes \tilde{x}_k^{(m)} + \delta_k^{(m)} \otimes (\tilde{x}_k^{(m)} - x_k^{(m)})\| \leq \|\tilde{\delta}_k^{(m)} - \delta_k^{(m)}\| \|\tilde{x}_k^{(m)}\| + \|\delta_k^{(m)}\| \|\tilde{x}_k^{(m)} - x_k^{(m)}\|. \end{aligned} \quad (50)$$

According to Lemma 8 and Lemma 5, it follows that

$$\begin{aligned} & \|\tilde{\nabla}_{W^{(m)}}^k f - \nabla_{W^{(m)}} f(W_k; \xi_k)\| \\ & \leq ((L_{g,0} W_{\max,2})^m C_\delta^{(m)} + (L_{g,0} W_{\max,2})^{M-m} L_{\ell,0} L_{g,0} C_x^{(m)}) \sum_{m'=1}^M \sum_{k'=k-(M-m')}^{k-1} \|\Delta_{k'}^{(m')}\| \\ & = C_f^{(m)} \sum_{m'=1}^M \sum_{k'=k-(M-m')}^{k-1} \|\Delta_{k'}^{(m')}\|. \end{aligned} \quad (51)$$

It completes the proof. \square

Bounds of delay errors. In Analog-SGD-AP, the computations in both the forward and backward passes involve stale weights, which introduce delay error in the signals. This section presents bounds on the delay error.

Lemma 7 (Lipschitz continuity of loss function). *There exists $L_{\ell,0}$ such that for any $m \in [M]$, $\|\nabla_{x^{(m)}}\ell(x_k^{(m)}, y_k)\| \leq L_{\ell,0}$ and $\|\nabla_{\tilde{x}^{(m)}}\ell(\tilde{x}_k^{(m)}, y_k)\| \leq L_{\ell,0}$.*

Proof. According to norm equivalence, there exists $W_{\max,2} = cW_{\max}$ with c is defined by the dimension of $W_k^{(m)}$, such that $\|W_k^{(m)}\| \leq W_{\max,2}$. For $m \in [M]$, according to the forward recursion (3), it holds that

$$\begin{aligned} \|x_k^{(m+1)}\| &\stackrel{(a)}{=} \|g^{(m)}(z_k^{(m)}) - g^{(m)}(0)\| \stackrel{(b)}{\leq} L_{g,0}\|z_k^{(m)}\| = L_{g,0}\|W_k^{(m)}x_k^{(m)}\| \\ &\leq L_{g,0}\|W_k^{(m)}\|\|x_k^{(m)}\| \leq L_{g,0}W_{\max,2}\|x_k^{(m)}\| \end{aligned} \quad (52)$$

where (a) and (b) hold because of Assumption 3 (1) and (2). Then by induction, we get $\|x_k^{(m)}\| \leq (L_{g,0}W_{\max,2})^m$ and the same bound holds for $\|\tilde{x}_k^{(m)}\|$. Since $\ell(\cdot, \cdot)$ is differentiable so that $\nabla\ell(\cdot, \cdot)$ is continuous, then there exists $L_{f,0}$ such that $\|\nabla_{x^{(m)}}\ell(x_k^{(m)}, y_k)\| \leq L_{f,0}$ and $\|\nabla_{\tilde{x}^{(m)}}\ell(\tilde{x}_k^{(m)}, y_k)\| \leq L_{f,0}$ hold for any $k, m \in [M]$. \square

Lemma 8 (boundeds signal). *Under Assumption 2–4, both forward and backward signals are bounded, i.e., $\forall m \in [M + 1]$*

$$\|x_k^{(m)}\| \leq (L_{g,0}W_{\max,2})^m, \quad \|\delta_k^{(m)}\| \leq (L_{g,0}W_{\max,2})^{M-m}L_{\ell,0}L_{g,0}, \quad (53)$$

$$\|\tilde{x}_k^{(m)}\| \leq (L_{g,0}W_{\max,2})^m, \quad \|\tilde{\delta}_k^{(m)}\| \leq (L_{g,0}W_{\max,2})^{M-m}L_{\ell,0}L_{g,0}. \quad (54)$$

Proof of Lemma 8. This lemma is proved by induction over m . The statement for $\|x_k^{(m)}\|$ and $\|\tilde{x}_k^{(m)}\|$ at $m = 1$ trivially hold because $x_k^{(0)} = \tilde{x}_k^{(0)} = x_k$. For $\|\delta_k^{(M+1)}\|$ and $\|\tilde{\delta}_k^{(M+1)}\|$, we have

$$\begin{aligned} \|\delta_k^{(M+1)}\| &= \|\nabla_{x^{(M+1)}}\ell(x_k^{(M+1)}, y_k)\nabla g^{(M)}(z_k^{(M)})\| \\ &\leq \|\nabla_{x^{(M+1)}}\ell(x_k^{(M+1)}, y_k)\|\|\nabla g^{(M)}(z_k^{(M)})\| \leq L_{\ell,0}L_{g,0} \end{aligned} \quad (55)$$

$$\begin{aligned} \|\tilde{\delta}_k^{(M+1)}\| &= \|\nabla_{x^{(M+1)}}\ell(\tilde{x}_k^{(M+1)}, y_k)\nabla g^{(M)}(\tilde{z}_k^{(M)})\| \\ &\leq \|\nabla_{x^{(M+1)}}\ell(\tilde{x}_k^{(M+1)}, y_k)\|\|\nabla g^{(M)}(\tilde{z}_k^{(M)})\| \leq L_{\ell,0}L_{g,0}. \end{aligned} \quad (56)$$

For $m \in [M]$, according to the forward recursion (3), it holds that

$$\begin{aligned} \|x_k^{(m+1)}\| &\stackrel{(a)}{=} \|g^{(m)}(z_k^{(m)}) - g^{(m)}(0)\| \stackrel{(b)}{\leq} L_{g,0} \|x_k^{(m)}\| = L_{g,0} \|W_k^{(m)} x_k^{(m)}\| \\ &\leq L_{g,0} \|W_k^{(m)}\| \|x_k^{(m)}\| \leq L_{g,0} W_{\max,2} \|x_k^{(m)}\| \end{aligned} \quad (57)$$

where (a) and (b) hold because of Assumption 3 (1) and (2). According to the backward recursion (4), it holds that

$$\begin{aligned} \|\delta_k^{(m)}\| &= \|\delta_k^{(m+1)} W_k^{(m+1)} \nabla g^{(m)}(z_k^{(m)})\| \\ &\leq \|\delta_k^{(m+1)}\| \|W_k^{(m+1)}\| \|\nabla g^{(m)}(z_k^{(m)})\| \leq L_{g,0} W_{\max,2} \|\delta_k^{(m+1)}\|, \end{aligned} \quad (58)$$

$$\begin{aligned} \|\tilde{\delta}_k^{(m)}\| &= \|\tilde{\delta}_k^{(m+1)} W_k^{(m+1)} \nabla g^{(m)}(\tilde{z}_k^{(m)})\| \\ &\leq \|\tilde{\delta}_k^{(m+1)}\| \|W_k^{(m+1)}\| \|\nabla g^{(m)}(\tilde{z}_k^{(m)})\| \leq L_{g,0} W_{\max,2} \|\tilde{\delta}_k^{(m+1)}\|. \end{aligned} \quad (59)$$

The proof has finished. \square

APPENDIX C

SMOOTHNESS OF THE OBJECT

This section proves Lemma 2, i.e. the object is L -smooth. Before that, we introduce a lemma as the step stone. Since the definition of function smoothness involves two weights W , W' and both of them generate a sequence of forward and backward signals, we require symbols to represent them. Using slightly abusing notation in this section, we denote the forward signals computed by W and \tilde{W} as $x^{(m)}$ and $\tilde{x}^{(m)}$, respectively, and denote the backward signals as $\delta^{(m)}$ and $\tilde{\delta}^{(m)}$, respectively.

Lemma 9 (Signal stability, restatement of Lemma 1). *Denote the forward signals computed by W and \tilde{W} as $x^{(m)}$ and $\tilde{x}^{(m)}$, respectively, and denote the backward signals as $\delta^{(m)}$ and $\tilde{\delta}^{(m)}$, respectively.*

$$\|\tilde{x}^{(m)} - x^{(m)}\|^2 \leq C_{x'}^{(m)} \|\tilde{W} - W\|^2, \quad (60)$$

$$\|\tilde{z}^{(m)} - z^{(m)}\|^2 \leq C_{z'}^{(m)} \|\tilde{W} - W\|^2, \quad (61)$$

$$\|\tilde{\delta}^{(m)} - \delta^{(m)}\|^2 \leq C_{\delta'}^{(m)} \|\tilde{W} - W\|^2, \quad (62)$$

where the constants $C_x^{(m)}$ and $C_z^{(m)}$ are defined by

$$C_{x'}^{(m)} := 2L_{g,0}(L_{g,0}W_{\max,2})^{2(m-1)}, \quad (63)$$

$$C_{z'}^{(m)} := 2(L_{g,0}W_{\max,2})^{2(m-1)}, \quad (64)$$

and $C_{\delta'}^{(m)}$ is defined by

$$\begin{aligned} C_{\delta'}^{(m)} &:= 3(L_{g,0}W_{\max,2})^2(2L_{\ell,1}^2L_{g,0}^4 + 2L_{\ell,0}^2L_{g,1}^2)(L_{g,0}W_{\max,2})^{2(M-1)} \\ &+ 3(L_{g,0}W_{\max,2})^{2(M-m)}L_{\ell,0}^2L_{g,0}^4 \sum_{m''=m}^{M-1} (L_{g,0}W_{\max,2})^{2(M-1-m'')} \frac{1 - (L_{g,0}W_{\max,2})^{2(M-m)}}{1 - L_{g,0}W_{\max,2}} \\ &+ 3(L_{g,0}W_{\max,2})^{2(M-1)}L_{\ell,0}^2L_{g,1}^2 \sum_{m''=m}^{M-1} (L_{g,0}W_{\max,2})^{2(M-1-m'')} \frac{1 - (L_{g,0}W_{\max,2})^{2(M-m)}}{1 - L_{g,0}W_{\max,2}}. \end{aligned} \quad (65)$$

Proof of Lemma 1 and Lemma 9. We first bound the delay of forward signal $\tilde{x}_k^{(m)}$. At the first layer, there is no delay, i.e. $\tilde{x}^{(1)} = x^{(1)} = x$. For other layers $m \geq 1$

$$\begin{aligned} \|\tilde{x}^{(m+1)} - x^{(m+1)}\|^2 &\leq L_{g,0}^2 \|\tilde{z}^{(m)} - z^{(m)}\|^2 \\ &= L_{g,0}^2 \|\tilde{W}^{(m)}\tilde{x}^{(m)} - W^{(m)}x^{(m)}\|^2 \\ &= L_{g,0}^2 \|(\tilde{W}^{(m)} - W^{(m)})\tilde{x}^{(m)} + W^{(m)}(\tilde{x}^{(m)} - x^{(m)})\|^2 \\ &\leq 2L_{g,0}^2 (\|\tilde{W}^{(m)} - W^{(m)}\|^2 \|\tilde{x}^{(m)}\|^2 + \|W^{(m)}\|^2 \|\tilde{x}^{(m)} - x^{(m)}\|^2) \\ &\leq 2L_{g,0}^2 ((L_{g,0}W_{\max,2})^{2m} \|\tilde{W}^{(m)} - W^{(m)}\|^2 + W_{\max,2}^2 \|\tilde{x}^{(m)} - x^{(m)}\|^2). \end{aligned} \quad (66)$$

Expanding inequality (66) from m to 1 and using the fact $\tilde{x}^{(1)} = x^{(1)} = x$ yield

$$\begin{aligned} \|\tilde{x}^{(m)} - x^{(m)}\|^2 &\leq 2L_{g,0}^2 (L_{g,0}W_{\max,2})^{2(m-1)} \|\tilde{W}^{(m-1)} - W^{(m-1)}\|^2 + 2L_{g,0}^2 W_{\max,2}^2 \|\tilde{x}^{(m-1)} - x^{(m-1)}\|^2 \\ &\leq 2L_{g,0}^2 \sum_{m'=2}^m (L_{g,0}W_{\max,2})^{2(m'-1)} (L_{g,0}W_{\max,2})^{2(m-m')} \|\tilde{W}^{(m'-1)} - W^{(m'-1)}\|^2 \\ &= 2L_{g,0}^2 (L_{g,0}W_{\max,2})^{2(m-1)} \sum_{m'=2}^m \|\tilde{W}^{(m'-1)} - W^{(m'-1)}\|^2 \\ &= 2L_{g,0}^2 (L_{g,0}W_{\max,2})^{2(m-1)} \sum_{m'=1}^{m-1} \|\tilde{W}^{(m')} - W^{(m')}\|^2 \end{aligned} \quad (67)$$

where the last equality reindexes the summation. By applying the relation

$$\sum_{m'=1}^{m-1} \|\tilde{W}^{(m')} - W^{(m')}\|^2 \leq \sum_{m'=1}^M \|\tilde{W}^{(m')} - W^{(m')}\|^2 = \|\tilde{W} - W\|^2 \quad (68)$$

we prove (60). Inferring in the similar way of (66)-(67), we obtain (61)

$$\|\tilde{z}^{(m)} - z^{(m)}\|^2 \leq 2(L_{g,0}W_{\max,2})^{2(m-1)}\|\tilde{W} - W\|^2 \quad (69)$$

We then bound the difference of the backward signal $\tilde{\delta}^{(m)}$ for $m \in [M-1]$

$$\begin{aligned} \|\tilde{\delta}^{(m)} - \delta^{(m)}\|^2 &= \|\tilde{\delta}^{(m+1)}\tilde{W}^{(m+1)}\nabla g^{(m)}(z^{(m)}) - \delta^{(m+1)}W^{(m+1)}\nabla g^{(m)}(z^{(m)})\|^2 \quad (70) \\ &\leq 3\|\tilde{\delta}^{(m+1)} - \delta^{(m+1)}\|^2\|\tilde{W}^{(m+1)}\|^2\|\nabla g^{(m)}(z^{(m)})\|^2 \\ &\quad + 3\|\delta^{(m+1)}\|^2\|\tilde{W}^{(m+1)} - W^{(m+1)}\|^2\|\nabla g^{(m)}(z^{(m)})\|^2 \\ &\quad + 3\|\delta^{(m+1)}\|^2\|W^{(m+1)}\|^2\|\nabla g^{(m)}(z^{(m)}) - \nabla g^{(m)}(\tilde{z}^{(m)})\|^2 \\ &\leq 3(L_{g,0}W_{\max,2})^2\|\tilde{\delta}^{(m+1)} - \delta^{(m+1)}\|^2 + 3(L_{g,0}W_{\max,2})^{2(M-m)}L_{\ell,0}^2L_{g,0}^4\|\tilde{W}^{(m+1)} - W^{(m+1)}\|^2 \\ &\quad + 3W_{\max,2}^2(L_{g,0}W_{\max,2})^{2(M-m-1)}L_{\ell,0}^2L_{g,0}^2L_{g,1}^2\|z^{(m)} - \tilde{z}^{(m)}\|^2 \end{aligned}$$

where the last inequality comes from Assumption 3 (1)-(2) and Lemma 8. Substituting (69) into (70), we can further bound (70) by

$$\begin{aligned} \|\tilde{\delta}^{(m)} - \delta^{(m)}\|^2 &\quad (71) \\ &\leq 3L_{g,0}^2W_{\max,2}^2\|\tilde{\delta}^{(m+1)} - \delta^{(m+1)}\|^2 + 3(L_{g,0}W_{\max,2})^{2(M-m)}L_{\ell,0}^2L_{g,0}^4\|\tilde{W}^{(m+1)} - W^{(m+1)}\|^2 \\ &\quad + 3W_{\max,2}^2(L_{g,0}W_{\max,2})^{2(M-m-1)}L_{\ell,0}^2L_{g,0}^2L_{g,1}^2(L_{g,0}W_{\max,2})^{2(m-1)}\sum_{m'=1}^{m-1}\|\tilde{W}^{(m')} - W^{(m')}\|^2 \\ &= 3L_{g,0}^2W_{\max,2}^2\|\tilde{\delta}^{(m+1)} - \delta^{(m+1)}\|^2 + 3(L_{g,0}W_{\max,2})^{2(M-m)}L_{\ell,0}^2L_{g,0}^4\|\tilde{W}^{(m+1)} - W^{(m+1)}\|^2 \\ &\quad + 3(L_{g,0}W_{\max,2})^{2(M-1)}L_{\ell,0}^2L_{g,1}^2\sum_{m'=1}^{m-1}\|\tilde{W}^{(m')} - W^{(m')}\|^2 \\ &\leq 3(L_{g,0}W_{\max,2})^{2(M-m)}\|\delta^{(M)} - \tilde{\delta}^{(M)}\|^2 \end{aligned}$$

$$\begin{aligned}
& + 3(L_{g,0}W_{\max,2})^{2(M-m)}L_{\ell,0}^2L_{g,0}^4 \sum_{m''=m}^{M-1} (L_{g,0}W_{\max,2})^{2(M-1-m'')} \|\tilde{W}^{(m''+1)} - W^{(m''+1)}\|^2 \\
& + 3(L_{g,0}W_{\max,2})^{2(M-1)}L_{\ell,0}^2L_{g,1}^2 \sum_{m''=m}^{M-1} (L_{g,0}W_{\max,2})^{2(M-1-m'')} \sum_{m'=1}^{m''-1} \|\tilde{W}^{(m')} - W^{(m')}\|^2.
\end{aligned}$$

To bound the first term in the RHS of (71), we manipulate the different $\|\delta^{(M)} - \tilde{\delta}^{(M)}\|$ by

$$\begin{aligned}
& \|\delta^{(M)} - \tilde{\delta}^{(M)}\|^2 \tag{72} \\
& = \|\nabla_{x^{(M+1)}}\ell(x^{(M+1)}, y)\nabla g^{(M)}(z^{(M)}) - \nabla_{x^{(M+1)}}\ell(\tilde{x}^{(M+1)}, y)\nabla g^{(M)}(\tilde{z}^{(M)})\|^2 \\
& \leq 2\|\nabla_{x^{(M+1)}}\ell(x^{(M+1)}, y) - \nabla_{x^{(M+1)}}\ell(\tilde{x}^{(M+1)}, y)\|^2\|\nabla g^{(M)}(z^{(M)})\|^2 \\
& \quad + 2\|\nabla_{x^{(M+1)}}\ell(\tilde{x}^{(M+1)}, y)\|^2\|\nabla g^{(M)}(\tilde{z}^{(M)}) - \nabla g^{(M)}(z^{(M)})\|^2 \\
& \stackrel{(a)}{\leq} 2L_{\ell,1}^2L_{g,0}^2\|x^{(M+1)} - \tilde{x}^{(M+1)}\|^2 + 2L_{\ell,0}^2L_{g,1}^2\|\tilde{z}^{(M)} - z^{(M)}\|^2 \\
& \leq (2L_{\ell,1}^2L_{g,0}^4 + 2L_{\ell,0}^2L_{g,1}^2)\|\tilde{z}^{(M)} - z^{(M)}\|^2 \\
& \leq (2L_{\ell,1}^2L_{g,0}^4 + 2L_{\ell,0}^2L_{g,1}^2)(L_{g,0}W_{\max,2})^{2(M-1)} \sum_{m'=1}^{M-1} \|\tilde{W}^{(m')} - W^{(m')}\|^2.
\end{aligned}$$

where (a) comes from Assumption 3 and Assumption 4.

To bound the second term in the RHS of (71), we add some terms into the summation

$$\begin{aligned}
& \sum_{m''=m}^{M-1} (L_{g,0}W_{\max,2})^{2(M-1-m'')} \|\tilde{W}^{(m''+1)} - W^{(m''+1)}\|^2 \tag{73} \\
& \leq \sum_{m''=m}^{M-1} (L_{g,0}W_{\max,2})^{2(M-1-m'')} \sum_{m'=1}^M \|\tilde{W}^{(m')} - W^{(m')}\|^2 \\
& = \frac{1 - (L_{g,0}W_{\max,2})^{2(M-m)}}{1 - L_{g,0}W_{\max,2}} \sum_{m'=1}^M \|\tilde{W}^{(m')} - W^{(m')}\|^2.
\end{aligned}$$

To bound the third term in the RHS of (71), we change the upper bound of the second summation from m'' to M and get

$$\begin{aligned}
& \sum_{m''=m}^{M-1} (L_{g,0}W_{\max,2})^{2(M-1-m'')} \sum_{m'=1}^{m''-1} \|\tilde{W}^{(m')} - W^{(m')}\|^2 \tag{74} \\
& \leq \sum_{m''=m}^{M-1} (L_{g,0}W_{\max,2})^{2(M-1-m'')} \sum_{m'=1}^M \|\tilde{W}^{(m')} - W^{(m')}\|^2
\end{aligned}$$

$$= \frac{1 - (L_{g,0}W_{\max,2})^{2(M-m)}}{1 - L_{g,0}W_{\max,2}} \sum_{m'=1}^M \|\tilde{W}^{(m')} - W^{(m')}\|^2.$$

Substituting (72)–(74) back into (71) we have

$$\|\tilde{\delta}^{(m)} - \delta^{(m)}\|^2 \leq C_{\delta'}^{(m)} \sum_{m'=1}^M \|\tilde{W}^{(m')} - W^{(m')}\|^2. \quad (75)$$

This completes the proof. \square

Lemma 10 (smoothness of the objective, restatement of Lemma 2). *Under Assumption 2–5, the objective is L -smooth with respect to W , i.e. $\forall \xi = (x, y) \in \mathcal{X} \times \mathcal{Y}$,*

$$\|\nabla f(W; \xi) - \nabla f(\tilde{W}; \xi)\| \leq L_f \|W - \tilde{W}\| \quad (76)$$

where the smoothness constant is defined as

$$L_f := \sqrt{2 \sum_{m=1}^M ((L_{g,0}W_{\max,2})^{2m} C_{\delta'}^{(m)} + (L_{g,0}W_{\max,2})^{2(M-m)} L_{\ell,0}^2 L_{g,0}^2 C_{x'}^{(m)})}. \quad (77)$$

Proof of Lemma 2 and Lemma 10. Analogous to the proof of Lemma (9), we use $x^{(m)}/\delta^{(m)}$ and $\tilde{x}^{(m)}/\tilde{\delta}^{(m)}$ to denote the forward/backward signals related to W and \tilde{W} , respectively. It follows by definition of gradient (5) that

$$\begin{aligned} \|\nabla f(W; \xi) - \nabla f(\tilde{W}; \xi)\|^2 &= \sum_{m=1}^M \|\nabla_{W^{(m)}} f(W; \xi) - \nabla_{W^{(m)}} f(\tilde{W}; \xi)\|^2 \\ &= \sum_{m=1}^M \|\tilde{\delta}^{(m)} \otimes \tilde{x}^{(m)} - \delta^{(m)} \otimes x^{(m)}\|^2 \\ &= \sum_{m=1}^M \|(\tilde{\delta}^{(m)} - \delta^{(m)}) \otimes \tilde{x}^{(m)} + \delta^{(m)} \otimes (\tilde{x}^{(m)} - x^{(m)})\|^2 \\ &\leq 2 \sum_{m=1}^M \|\tilde{\delta}^{(m)} - \delta^{(m)}\|^2 \|\tilde{x}^{(m)}\|^2 + 2 \|\delta^{(m)}\|^2 \|\tilde{x}^{(m)} - x^{(m)}\|^2. \end{aligned} \quad (78)$$

According to Lemma 8 and Lemma 9, it follows that

$$\|\nabla f(W; \xi) - \nabla f(\tilde{W}; \xi)\|^2 \quad (79)$$

$$\begin{aligned}
&\leq 2 \sum_{m=1}^M ((L_{g,0} W_{\max,2})^{2m} C_{\delta'}^{(m)} + (L_{g,0} W_{\max,2})^{2(M-m)} L_{\ell,0}^2 L_{g,0}^2 C_{x'}^{(m)}) \|\tilde{W} - W\|^2 \\
&= L_f^2 \|\tilde{W} - W\|^2.
\end{aligned}$$

Taking the square root on both sides of (79) completes the proof. \square

APPENDIX D

PROOF OF THEOREM 1: ANALOG SGD WITH SYNCHRONOUS PIPELINE

This section provides the convergence guarantee of the Analog SGD with synchronous pipeline, whose iteration is

$$W_{k,b+1}^{(m)} = W_{k,b}^{(m)} - \frac{\alpha}{B} \nabla_{W^{(m)}} f(W_k; \xi_{k,b}) - \frac{\alpha}{\tau B} |\nabla_{W^{(m)}} f(W_k; \xi_{k,b})| \odot W_{k,b}^{(m)}. \quad (80)$$

Theorem 1 (Iteration complexity, Analog-SGD-SP). *Under Assumption 1–5, if the learning rate is set as $\alpha = \sqrt{\frac{B(f(W_0) - f^*)}{\sigma^2 L_f K}}$ and K is sufficiently large such that $\alpha \leq \frac{1}{L}$, it holds that*

$$E_K \leq 4 \sqrt{\frac{(f(W_0) - f^*) \sigma^2 L_f}{BK}} \frac{1}{1 - W_{\max,\infty}^2 / \tau^2} + \sigma^2 S$$

where B is the number of micro-batches, and the constant S is given by $S := \frac{W_{\max,\infty} / \tau^2}{1 - W_{\max,\infty} / \tau^2}$.

Proof of Theorem 1. Denote the average gradient by

$$\bar{\nabla} f(W_k; \xi_k) := \frac{1}{B} \sum_{b=1}^B \nabla f(W_k; \xi_{k,b}), \quad (81)$$

which satisfies that $\mathbb{E}_{\{\xi_{k,b}, b \in [B]\}} [\bar{\nabla} f(W_k; \xi_k)] = \nabla f(W_k)$. Furthermore, the independence of sampling (c.f. Assumption 1) ensures that

$$\begin{aligned}
&\mathbb{E}_{\{\xi_{k,b}, b \in [B]\}} [\|\bar{\nabla} f(W_k; \xi_k) - \nabla f(W_k)\|^2] \\
&= \mathbb{E}_{\{\xi_{k,b}, b \in [B]\}} [\|\frac{1}{B} \sum_{b=1}^B \nabla f(W_k; \xi_{k,b}) - \nabla f(W_k)\|^2] \\
&= \frac{1}{B^2} \sum_{b=1}^B \mathbb{E}_{\xi_{k,b}} [\|\nabla f(W_k; \xi_{k,b}) - \nabla f(W_k)\|^2] \leq \sigma^2 / B.
\end{aligned} \quad (82)$$

The L -smooth assumption of the objective (c.f. Lemma 10) implies that

$$\begin{aligned}
& \mathbb{E}_{\{\xi_k, b: b \in [B]\}} [f(W_{k+1})] \\
& \leq f(W_k) + \mathbb{E}_{\{\xi_k, b: b \in [B]\}} [\langle \nabla f(W_k), W_{k+1} - W_k \rangle] + \frac{L_f}{2} \mathbb{E}_{\{\xi_k, b: b \in [B]\}} [\|W_{k+1} - W_k\|^2] \\
& \leq f(W_k) - \frac{\alpha}{2} \|\nabla f(W_k)\|^2 - \left(\frac{1}{2\alpha} - L_f\right) \mathbb{E}_{\varepsilon_k} [\|W_{k+1} - W_k + \alpha(\bar{\nabla} f(W_k; \xi_k) - \nabla f(W_k))\|^2] \\
& \quad + \alpha^2 L_f \mathbb{E}_{\varepsilon_k} [\|\bar{\nabla} f(W_k; \xi_k) - \nabla f(W_k)\|^2] + \frac{1}{2\alpha} \|W_{k+1} - W_k + \alpha(\nabla f(W_k) + \varepsilon_k)\|^2
\end{aligned} \tag{83}$$

where the second inequality comes from the assumption that the expectation of the noise is 0 (Assumption 1)

$$\begin{aligned}
& \mathbb{E}_{\varepsilon_k} [\langle \nabla f(W_k), W_{k+1} - W_k \rangle] \\
& = \mathbb{E}_{\varepsilon_k} [\langle \nabla f(W_k), W_{k+1} - W_k + \alpha(\bar{\nabla} f(W_k; \xi_k) - \nabla f(W_k)) \rangle] \\
& = -\frac{\alpha}{2} \|\nabla f(W_k)\|^2 - \frac{1}{2\alpha} \mathbb{E}_{\varepsilon_k} [\|W_{k+1} - W_k + \alpha(\bar{\nabla} f(W_k; \xi_k) - \nabla f(W_k))\|^2] \\
& \quad + \frac{1}{2\alpha} \mathbb{E}_{\varepsilon_k} [\|W_{k+1} - W_k + \alpha \bar{\nabla} f(W_k; \xi_k)\|^2]
\end{aligned} \tag{84}$$

and the following inequality

$$\begin{aligned}
\frac{L_f}{2} \mathbb{E}_{\varepsilon_k} [\|W_{k+1} - W_k\|^2] & \leq L_f \mathbb{E}_{\{\xi_k, b: b \in [B]\}} [\|W_{k+1} - W_k + \alpha(\bar{\nabla} f(W_k; \xi_k) - \nabla f(W_k))\|^2] \\
& \quad + \alpha^2 L \mathbb{E}_{\{\xi_k, b: b \in [B]\}} [\|\bar{\nabla} f(W_k; \xi_k) - \nabla f(W_k)\|^2].
\end{aligned} \tag{85}$$

With the learning rate $\alpha \leq \frac{1}{2L}$ and bounded variance (c.f. (82)), (83) becomes

$$\mathbb{E}_{\{\xi_k, b: b \in [B]\}} [f(W_{k+1})] \leq f(W_k) - \frac{\alpha}{2} \|\nabla f(W_k)\|^2 + \frac{\alpha^2 L_f \sigma^2}{B} \tag{86}$$

$$+ \frac{1}{2\alpha} \mathbb{E}_{\{\xi_k, b: b \in [B]\}} [\|W_{k+1} - W_k + \alpha \bar{\nabla} f(W_k; \xi_k)\|^2]. \tag{87}$$

According the dynamics of Analog-SGD-SP, the last term in the RHS of (86) is bounded by

$$\begin{aligned}
& \frac{1}{2\alpha} \mathbb{E}_{\{\xi_k, b: b \in [B]\}} [\|W_{k+1} - W_k + \alpha \bar{\nabla} f(W_k; \xi_k)\|^2] \\
& = \frac{\alpha}{2\tau^2} \mathbb{E}_{\{\xi_k, b: b \in [B]\}} \left[\left\| \frac{1}{B} \sum_{b=1}^B |\nabla f(W_k; \xi_{k,b})| \odot W_{k,b} \right\|^2 \right]
\end{aligned} \tag{88}$$

$$\begin{aligned}
&\leq \frac{\alpha}{2\tau^2} \frac{1}{B} \sum_{b=1}^B \mathbb{E}_{\xi_{k,b}} [\|\nabla f(W_k; \xi_{k,b}) \odot W_{k,b}\|^2] \\
&\leq \frac{\alpha}{2\tau^2} \max_{b \in [B]} \|W_{k,b}\|_\infty^2 \frac{1}{B} \sum_{b=1}^B \mathbb{E}_{\xi_{k,b}} [\|\nabla f(W_k; \xi_{k,b})\|^2].
\end{aligned}$$

By the variance decomposition and Assumption 1, the term above can be bounded by

$$\mathbb{E}_{\xi_{k,b}} [\|f(W_k; \xi_{k,b})\|^2] = \|\nabla f(W_k)\|^2 + \mathbb{E}_{\xi_k} [\|\nabla f(W_k; \xi_{k,b}) - \nabla f(W_k)\|^2] \leq \|\nabla f(W_k)\|^2 + \sigma^2. \quad (89)$$

Consequently, combining (86), (88) and (89) yields

$$\begin{aligned}
&\mathbb{E}_{\{\xi_{k,b}: b \in [B]\}} [f(W_{k+1})] \\
&\leq f(W_k) - \frac{\alpha}{2} \left(1 - \frac{\max_{b \in [B]} \|W_{k,b}\|_\infty^2}{\tau^2}\right) \|\nabla f(W_k)\|^2 + \frac{\alpha^2 L_f \sigma^2}{B} + \frac{\alpha \sigma^2}{2\tau^2} \max_{b \in [B]} \|W_{k,b}\|_\infty^2.
\end{aligned} \quad (90)$$

Organizing the terms, taking expectation, averaging (90) over k from 0 to $K-1$, we obtain

$$\begin{aligned}
\frac{1}{K} \sum_{k=0}^{K-1} \mathbb{E} [\|\nabla f(W_k)\|^2] &\leq \frac{2(f(W_0) - \mathbb{E}[f(W_{k+1})])}{1 - W_{\max, \infty}^2 / \tau^2} + \frac{\alpha L_f \sigma^2}{B(1 - W_{\max, \infty}^2 / \tau^2)} \\
&\quad + \frac{\sigma^2}{K} \sum_{k=0}^{K-1} \frac{\max_{b \in [B]} \|W_{k,b}\|_\infty^2 / \tau^2}{1 - \max_{b \in [B]} \|W_{k,b}\|_\infty^2 / \tau^2}. \\
&\leq 4 \sqrt{\frac{(f(W_0) - f^*) \sigma^2 L_f}{BK}} \frac{1}{1 - W_{\max, \infty}^2 / \tau^2} + \sigma^2 S_K
\end{aligned} \quad (91)$$

where the second inequality uses $f(W_{k+1}) \geq f^*$ and specifies $\alpha = \sqrt{\frac{B(f(W_0) - f^*)}{\sigma^2 L_f K}}$. Now we complete the proof. \square

APPENDIX E

PROOF OF THEOREM 2: ANALOG SGD WITH ASYNCHRONOUS PIPELINE

This section provides the convergence guarantee of the Analog SGD under non-convex assumption on asymmetric linear devices.

Theorem 2 (Iteration complexity, Analog-SGD-AP). *Under Assumption 1–5, if the learning*

rate is set as $\alpha = \sqrt{\frac{f(W_0) - f^*}{\sigma^2 L_f K}}$ and K is sufficiently large such that $\alpha \leq \frac{1}{L_f}$, it holds that

$$E_K \leq 4\sqrt{\frac{(f(W_0) - f^*)\sigma^2 L_f}{K}} \frac{1}{1 - (1+u)W_{\max, \infty}^2/\tau^2} + \sigma^2 S' + \mathcal{O}\left(\frac{1+1/u}{K}\right) \quad (12)$$

where $u > 0$ is any number and S' denotes the amplification factor given by $S' := \frac{(1+u)W_{\max}^2/\tau^2}{1 - (1+u)W_{\max}^2/\tau^2}$.

Proof of Theorem 2. The L -smooth assumption of the objective (c.f. Lemma 10) implies that

$$\begin{aligned} & \mathbb{E}_{\xi_k}[f(W_{k+1})] \quad (92) \\ & \leq f(W_k) + \mathbb{E}_{\xi_k}[\langle \nabla f(W_k), W_{k+1} - W_k \rangle] + \frac{L_f}{2} \mathbb{E}_{\xi_k}[\|W_{k+1} - W_k\|^2] \\ & \leq f(W_k) - \frac{\alpha}{2} \|\nabla f(W_k)\|^2 - \left(\frac{1}{2\alpha} - L_f\right) \mathbb{E}_{\xi_k}[\|W_{k+1} - W_k + \alpha(\nabla f(W_k; \xi_k) - \nabla f(W_k))\|^2] \\ & \quad + \alpha^2 L_f \mathbb{E}_{\xi_k}[\|\nabla f(W_k; \xi_k) - \nabla f(W_k)\|^2] + \frac{1}{2\alpha} \mathbb{E}_{\xi_k}[\|W_{k+1} - W_k + \alpha \nabla f(W_k; \xi_k)\|^2] \end{aligned}$$

where the second inequality comes from the assumption that the expectation of the noise is 0 (Assumption 1)

$$\begin{aligned} & \mathbb{E}_{\xi_k}[\langle \nabla f(W_k), W_{k+1} - W_k \rangle] \quad (93) \\ & = \mathbb{E}_{\xi_k}[\langle \nabla f(W_k), W_{k+1} - W_k + \alpha(\nabla f(W_k; \xi_k) - \nabla f(W_k)) \rangle] \\ & = -\frac{\alpha}{2} \|\nabla f(W_k)\|^2 - \frac{1}{2\alpha} \mathbb{E}_{\xi_k}[\|W_{k+1} - W_k + \alpha(\nabla f(W_k; \xi_k) - \nabla f(W_k))\|^2] \\ & \quad + \frac{1}{2\alpha} \mathbb{E}_{\xi_k}[\|W_{k+1} - W_k + \alpha \nabla f(W_k; \xi_k)\|^2] \end{aligned}$$

and the following inequality

$$\begin{aligned} \frac{L_f}{2} \mathbb{E}_{\xi_k}[\|W_{k+1} - W_k\|^2] & \leq L_f \mathbb{E}_{\xi_k}[\|W_{k+1} - W_k + \alpha(\nabla f(W_k; \xi_k) - \nabla f(W_k))\|^2] \quad (94) \\ & \quad + \alpha^2 L_f \mathbb{E}_{\xi_k}[\|\nabla f(W_k; \xi_k) - \nabla f(W_k)\|^2]. \end{aligned}$$

With the learning rate $\alpha \leq \frac{1}{4L_f}$ and bounded variance of noise (Assumption 1), (92) becomes

$$\begin{aligned} \mathbb{E}_{\xi_k}[f(W_{k+1})] & \leq f(W_k) - \frac{\alpha}{2} \|\nabla f(W_k)\|^2 + \alpha^2 L_f \sigma^2 + \frac{1}{2\alpha} \mathbb{E}_{\xi_k}[\|W_{k+1} - W_k + \alpha \nabla f(W_k; \xi_k)\|^2] \\ & \quad - \frac{1}{4\alpha} \mathbb{E}_{\xi_k}[\|W_{k+1} - W_k + \alpha(\nabla f(W_k; \xi_k) - \nabla f(W_k))\|^2]. \quad (95) \end{aligned}$$

By the dynamics of Analog SGD, the last in the RHS of (95) is bounded by

$$\begin{aligned}
& \frac{1}{2\alpha} \mathbb{E}_{\xi_k} [\|W_{k+1} - W_k + \alpha \nabla f(W_k; \xi_k)\|^2] \\
&= \frac{\alpha}{2} \mathbb{E}_{\xi_k} [\|\tilde{\nabla}^k f - \nabla f(W_k; \xi_k) + \frac{1}{\tau} |\tilde{\nabla}^k f| \odot W_k\|^2] \\
&= \frac{\alpha}{2} \mathbb{E}_{\xi_k} [\|\tilde{\nabla}^k f - \nabla f(W_k; \xi_k) + \frac{1}{\tau} \tilde{\nabla}^k f \odot \text{sign}(\tilde{\nabla}^k f) \odot W_k\|^2] \\
&= \frac{\alpha}{2} \mathbb{E}_{\xi_k} [\|\tilde{\nabla}^k f - \nabla f(W_k; \xi_k) + \frac{1}{\tau} (\tilde{\nabla}^k f - \nabla f(W_k; \xi_k)) \odot \text{sign}(\tilde{\nabla}^k f) \odot W_k \\
&\quad + \frac{1}{\tau} \nabla f(W_k; \xi_k) \odot \text{sign}(\tilde{\nabla}^k f) \odot W_k\|^2] \\
&= \frac{\alpha}{2} \mathbb{E}_{\xi_k} [\|(\mathbf{1} + \frac{1}{\tau} \odot \text{sign}(\tilde{\nabla}^k f) \odot W_k) (\tilde{\nabla}^k f - \nabla f(W_k; \xi_k)) \\
&\quad + \frac{1}{\tau} \nabla f(W_k; \xi_k) \odot \text{sign}(\tilde{\nabla}^k f) \odot W_k\|^2]
\end{aligned} \tag{96}$$

where $\mathbf{1}$ is the all-one vector. Using inequality $\|x + y\|^2 \leq (1 + \frac{1}{u})\|x\|^2 + (1 + u)\|y\|^2$ we obtain

$$\begin{aligned}
& \frac{1}{2\alpha} \mathbb{E}_{\xi_k} [\|W_{k+1} - W_k + \alpha \nabla f(W_k; \xi_k)\|^2] \\
&\leq \frac{\alpha}{2} (1 + \frac{1}{u}) \mathbb{E}_{\xi_k} [\|(\mathbf{1} + \frac{1}{\tau} \odot \text{sign}(\tilde{\nabla}^k f) \odot W_k) \odot (\tilde{\nabla}^k f - \nabla f(W_k; \xi_k))\|^2] \\
&\quad + \frac{\alpha}{2\tau^2} (1 + u) \mathbb{E}_{\xi_k} [\|\nabla f(W_k; \xi_k) \odot \text{sign}(\tilde{\nabla}^k f) \odot W_k\|^2]
\end{aligned} \tag{97}$$

The first term in the RHS of (97) is bounded by

$$\begin{aligned}
& \frac{\alpha}{2} (1 + \frac{1}{u}) \mathbb{E}_{\xi_k} [\|(\mathbf{1} + \frac{1}{\tau} \odot \text{sign}(\tilde{\nabla}^k f) \odot W_k) \odot (\tilde{\nabla}^k f - \nabla f(W_k; \xi_k))\|^2] \\
&\leq \frac{\alpha}{2} (1 + \frac{1}{u}) \mathbb{E}_{\xi_k} [\|\mathbf{1} + \frac{1}{\tau} \odot \text{sign}(\tilde{\nabla}^k f) \odot W_k\|_\infty^2 \|\tilde{\nabla}^k f - \nabla f(W_k; \xi_k)\|^2] \\
&\leq \frac{\alpha}{2} (1 + \frac{1}{u}) (1 + W_{\max, \infty} / \tau)^2 \mathbb{E}_{\xi_k} [\|\tilde{\nabla}^k f - \nabla f(W_k; \xi_k)\|^2] \\
&\leq \frac{\alpha}{2} (1 + \frac{1}{u}) (1 + W_{\max, \infty} / \tau)^2 M^2 C_f^2 \mathbb{E}_{\xi_k} \left[\sum_{m'=1}^M \sum_{k'=k-(M-m')}^{k-1} \|\Delta_{k'}^{(m')}\|^2 \right].
\end{aligned} \tag{98}$$

where the last inequality comes from Lemma 6.

The second term in the RHS of (97) is bounded by

$$\begin{aligned}
& \frac{\alpha}{2\tau^2} (1 + u) \mathbb{E}_{\xi_k} [\|\nabla f(W_k; \xi_k) \odot \text{sign}(\tilde{\nabla}^k f) \odot W_k\|^2] \\
&\leq \frac{\alpha}{2\tau^2} (1 + u) \mathbb{E}_{\xi_k} [\|\nabla f(W_k; \xi_k)\|^2] \|W_k\|_\infty^2
\end{aligned} \tag{99}$$

$$\leq \frac{\alpha}{2\tau^2}(1+u)\|\nabla f(W_k)\|^2\|W_k\|_\infty^2 + \frac{\alpha\sigma^2}{2\tau^2}(1+u)\|W_k\|_\infty^2$$

where the last inequality comes from Assumption 1

$$\begin{aligned} \mathbb{E}_{\xi_k}[\|\nabla f(W_k; \xi_k)\|^2] &= \|\nabla f(W_k)\|^2 + \mathbb{E}_{\xi_k}[\|\nabla f(W_k; \xi_k) - \nabla f(W_k)\|^2] \\ &\leq \|\nabla f(W_k)\|^2 + \sigma^2. \end{aligned} \quad (100)$$

Plugging (97), (98) and (99) back into (96), we have

$$\begin{aligned} &\frac{1}{2\alpha}\mathbb{E}_{\xi_k}[\|W_{k+1} - W_k + \alpha\nabla f(W_k; \xi_k)\|^2] \\ &= \frac{\alpha}{2}\left(1 + \frac{1}{u}\right)(1 + W_{\max, \infty}/\tau)^2 C_f^2 M^2 \sum_{m'=1}^M \sum_{k'=k-(M-m')}^{k-1} \mathbb{E}_{\xi_k}[\|\Delta_{k'}^{(m')}\|^2] \\ &\quad + \frac{\alpha}{2\tau^2}(1+u)\|\nabla f(W_k)\|^2\|W_k\|_\infty^2 + \frac{\alpha\sigma^2}{2\tau^2}(1+u)\|W_k\|_\infty^2. \end{aligned} \quad (101)$$

Substituting (101) into (95) yields

$$\begin{aligned} &\mathbb{E}_{\xi_k}[f(W_{k+1})] \\ &\leq f(W_k) - \frac{\alpha}{2}\|\nabla f(W_k)\|^2 + \alpha^2 L_f \sigma^2 + \frac{\alpha}{2\tau^2}(1+u)\|\nabla f(W_k)\|^2\|W_k\|_\infty^2 + \frac{\alpha\sigma^2}{2\tau^2}(1+u)\|W_k\|_\infty^2 \\ &\quad - \frac{1}{4\alpha}\mathbb{E}_{\xi_k}[\|W_{k+1} - W_k + \alpha(\nabla f(W_k; \xi_k) - \nabla f(W_k))\|^2] \\ &\quad + \frac{\alpha}{2}\left(1 + \frac{1}{u}\right)(1 + W_{\max, \infty}/\tau)^2 C_f^2 M^2 \sum_{m'=1}^M \sum_{k'=k-(M-m')}^{k-1} \mathbb{E}_{\xi_k}[\|\Delta_{k'}^{(m')}\|^2]. \\ &= f(W_k) - \frac{\alpha}{2}\left(1 - (1+u)\frac{\|W_k\|_\infty^2}{\tau^2}\right)\|\nabla f(W_k)\|^2 + \alpha^2 L_f \sigma^2 + \frac{\alpha\sigma^2}{2\tau^2}(1+u)\|W_k\|_\infty^2 \\ &\quad - \frac{1}{4\alpha}\mathbb{E}_{\xi_k}[\|W_{k+1} - W_k + \alpha(\nabla f(W_k; \xi_k) - \nabla f(W_k))\|^2] \\ &\quad + \frac{\alpha}{2}\left(1 + \frac{1}{u}\right)(1 + W_{\max, \infty}/\tau)^2 C_f^2 M^2 \underbrace{\mathbb{E}_{\xi_k}\left[\sum_{m'=1}^M \sum_{k'=k-(M-m')}^{k-1} \|\Delta_{k'}^{(m')}\|^2\right]}_{=: \psi_k}. \end{aligned} \quad (102)$$

To deal with ψ_k in the RHS of (102), we define an auxiliary function

$$\Psi_k := \sum_{m'=1}^M \sum_{k'=k-(M-m')}^{k-1} (k' - k + M) \|\Delta_{k'}^{(m')}\|^2 \quad (103)$$

which has the following recursion from k to $k + 1$

$$\begin{aligned}
\Psi_{k+1} &= \sum_{m'=1}^M \sum_{k'=k+1-(M-m')}^k (k' - (k+1) + M) \|\Delta_{k'}^{(m')}\|^2 \\
&= \sum_{m'=1}^M \sum_{k'=k+1-(M-m')}^k (k' - k + M) \|\Delta_{k'}^{(m')}\|^2 - \sum_{m'=1}^M \sum_{k'=k+1-(M-m')}^k \|\Delta_{k'}^{(m')}\|^2 \\
&= \sum_{m'=1}^M \sum_{k'=k-(M-m')}^{k-1} (k' - k + M) \|\Delta_{k'}^{(m')}\|^2 - \sum_{m'=1}^M \sum_{k'=k+1-(M-m')}^k \|\Delta_{k'}^{(m')}\|^2 \\
&\quad + M \sum_{m'=1}^M \|\Delta_k^{(m')}\|^2 - \sum_{m'=1}^M m' \|\Delta_{k-(M-m')}^{(m')}\|^2 \\
&\leq \Psi_k - \psi_k + M \|W_{k+1} - W_k\|^2
\end{aligned} \tag{104}$$

where the last inequality holds by definition of $\Delta_k^{(m')}$, i.e.,

$$\sum_{m'=1}^M \|\Delta_k^{(m')}\|^2 = \sum_{m'=1}^M \|W_{k+1}^{(m')} - W_k^{(m')}\|^2 = \|W_{k+1} - W_k\|^2. \tag{105}$$

Construct a Lyapunov function by

$$\mathbb{V}_k := f(W_k) - f^* + \frac{\alpha}{2} \left(1 + \frac{1}{u}\right) (1 + W_{\max, \infty} / \tau)^2 C_f^2 M^2 \Psi_k. \tag{106}$$

According to (102), we have

$$\begin{aligned}
\mathbb{E}_{\xi_k} [\mathbb{V}_{k+1}] &= f(W_{k+1}) - f^* + \frac{\alpha}{2} \left(1 + \frac{1}{u}\right) (1 + W_{\max, \infty} / \tau)^2 C_f^2 M^2 \Psi_{k+1} \\
&\leq f(W_k) - \frac{\alpha}{2} \left(1 - (1+u) \frac{\|W_k\|_\infty^2}{\tau^2}\right) \|\nabla f(W_k)\|^2 + \alpha^2 L_f \sigma^2 + \frac{\alpha \sigma^2}{2\tau^2} (1+u) \|W_k\|_\infty^2 \\
&\quad - \frac{1}{4\alpha} \mathbb{E}_{\xi_k} [\|W_{k+1} - W_k + \alpha(\nabla f(W_k; \xi_k) - \nabla f(W_k))\|^2] \\
&\quad + \frac{\alpha}{2} \left(1 + \frac{1}{u}\right) (1 + W_{\max, \infty} / \tau)^2 C_f^2 M^3 \sum_{m'=1}^M \mathbb{E}_{\xi_k} [\|\Delta_{k'}^{(m')}\|^2].
\end{aligned} \tag{107}$$

we bound the last term of the RHS of (107) by

$$\begin{aligned}
&\|W_{k+1} - W_k\|^2 \\
&\leq 2\|W_{k+1} - W_k + \alpha(\nabla f(W_k; \xi_k) - \nabla f(W_k))\|^2 + 2\alpha^2 \|\nabla f(W_k; \xi_k) - \nabla f(W_k)\|^2
\end{aligned} \tag{108}$$

$$\leq 2\|W_{k+1} - W_k + \alpha(\nabla f(W_k; \xi_k) - \nabla f(W_k))\|^2 + 2\alpha^2\sigma^2.$$

Organizing the terms of (107), we obtain

$$\begin{aligned} & \frac{\alpha}{2} \left(1 - (1+u) \frac{\|W_k\|_\infty^2}{\tau^2} \right) \|\nabla f(W_k)\|^2 \\ & \leq \mathbb{V}_k - \mathbb{E}_{\xi_k}[\mathbb{V}_{k+1}] + \alpha^2 L_f \sigma^2 + \frac{\alpha \sigma^2}{2\tau^2} (1+u) \|W_k\|_\infty^2 \\ & \quad - \left(\frac{1}{4\alpha} - \alpha \left(1 + \frac{1}{u} \right) (1 + W_{\max, \infty} / \tau)^2 C_f^2 M^2 \right) \mathbb{E}_{\xi_k} [\|W_{k+1} - W_k + \alpha(\nabla f(W_k; \xi_k) - \nabla f(W_k))\|^2] \\ & \quad + \alpha^3 \left(1 + \frac{1}{u} \right) (1 + W_{\max, \infty} / \tau)^2 C_f^2 M^3 \sigma^2. \end{aligned} \tag{109}$$

Taking expectation, averaging (109) over k from 0 to $K-1$, and choosing the stepsize $\alpha \leq$

$\frac{1}{2\sqrt{1+1/u}(1+W_{\max, \infty}/\tau)C_f M}$ yield

$$\begin{aligned} & \frac{1}{K} \sum_{k=0}^{K-1} \mathbb{E} [\|\nabla f(W_k)\|^2] \\ & \leq \frac{2(\mathbb{V}_0 - \mathbb{E}[\mathbb{V}_{k+1}])}{\alpha K (1 - (1+u)W_{\max, \infty}^2/\tau^2)} + \frac{2\alpha L_f \sigma^2}{1 - (1+u)W_{\max, \infty}^2/\tau^2} \\ & \quad + \sigma^2 \frac{1}{K} \sum_{k=0}^{K-1} \frac{(1+u)\|W_k\|_\infty^2/\tau}{1 - (1+u)\|W_k\|_\infty^2/\tau^2} + \frac{\alpha^2(1+1/u)(1+W_{\max, \infty}/\tau)^4 C_f^2 M^3 \sigma^2}{(1 - (1+u)W_{\max, \infty}^2/\tau^2)}. \end{aligned} \tag{110}$$

Using the fact that $V_k \geq 0$ for any $k \in \mathbb{N}$ and $V_0 = f(W_0) - f^*$, and choosing the learning rate $\alpha = \sqrt{\frac{f(W_0) - f^*}{\sigma^2 L_f K}}$, we have

$$\begin{aligned} & \frac{1}{K} \sum_{k=0}^{K-1} \mathbb{E} [\|\nabla f(W_k)\|^2] \\ & \leq 4\sqrt{\frac{(f(W_0) - f^*)\sigma^2 L_f}{K}} \frac{1}{1 - (1+u)W_{\max, \infty}^2/\tau^2} + \sigma^2 S'_K + \mathcal{O}\left(\frac{1+1/u}{K}\right). \end{aligned} \tag{111}$$

where S'_K denotes the amplification factor given by

$$S'_K := \frac{1}{K} \sum_{k=0}^{K-1} \frac{(1+u)\|W_k\|_\infty^2/\tau^2}{1 - (1+u)\|W_k\|_\infty^2/\tau^2} \leq \frac{(1+u)W_{\max, \infty}^2/\tau^2}{1 - (1+u)W_{\max, \infty}^2/\tau^2}. \tag{112}$$

The proof is completed now. \square

APPENDIX F

CONVERGENCE OF DIGITAL ASYNCHRONOUS PIPELINE SGD

Theorem 3 (Iteration complexity, asynchronous pipeline). *Under Assumption 1–5, if the learning rate is set as $\alpha = \sqrt{\frac{f(W_0) - f^*}{\sigma^2 L_f K}}$ and K is sufficiently large such that $\alpha \leq \sqrt{\frac{1}{4C_f M^3}}$, it holds that*

$$\frac{1}{K} \sum_{k=0}^{K-1} \mathbb{E} [\|\nabla f(W_k)\|^2] \leq 4\sqrt{\frac{(f(W_0) - f^*)L_f\sigma^2}{K}} + \frac{2C_f M^3(f(W_0) - f^*)}{K L_f}. \quad (113)$$

Proof. The validation of inequality (92) does not rely on any training algorithm, and hence it still holds here. To bound the last term in the RHS of (92), we have

$$\begin{aligned} & \frac{1}{2\alpha} \mathbb{E}_{\xi_k} [\|W_{k+1} - W_k + \alpha \nabla f(W_k; \xi_k)\|^2] = \frac{\alpha}{2} \mathbb{E}_{\xi_k} [\|\tilde{\nabla}^k f - \nabla f(W_k; \xi_k)\|^2] \\ & \leq \frac{\alpha C_f}{2} \mathbb{E}_{\xi_k} \left[\sum_{m'=1}^M \sum_{k'=k-(M-m'+1)}^{k-1} \|\Delta_{k'}^{(m')}\|^2 \right] \leq \frac{\alpha C_f M^2}{2} \sum_{m'=1}^M \sum_{k'=k-(M-m'+1)}^{k-1} \mathbb{E}_{\xi_k} [\|\Delta_{k'}^{(m')}\|^2] \end{aligned} \quad (114)$$

where the first inequality is according to Lemma 6.

According to the descent lemma in (95), we have

$$\begin{aligned} & \mathbb{E}_{\xi_k} [f(W_{k+1})] \quad (115) \\ & \leq f(W_k) - \frac{\alpha}{2} \|\nabla f(W_k)\|^2 + \alpha^2 L_f \sigma^2 + \frac{1}{2\alpha} \mathbb{E}_{\xi_k} [\|W_{k+1} - W_k + \alpha \nabla f(W_k; \xi_k)\|^2] \\ & \quad - \frac{1}{4\alpha} \mathbb{E}_{\xi_k} [\|W_{k+1} - W_k + \alpha(\nabla f(W_k; \xi_k) - \nabla f(W_k))\|^2] \\ & \leq f(W_k) - \frac{\alpha}{2} \|\nabla f(W_k)\|^2 + \alpha^2 L_f \sigma^2 + \frac{\alpha C_f M^2}{2} \sum_{m'=1}^M \sum_{k'=k-(M-m'+1)}^{k-1} \mathbb{E}_{\xi_k} [\|\Delta_{k'}^{(m')}\|^2] \\ & \quad - \frac{1}{4\alpha} \mathbb{E}_{\xi_k} [\|W_{k+1} - W_k + \alpha(\nabla f(W_k; \xi_k) - \nabla f(W_k))\|^2] \end{aligned}$$

where the second inequality is earned by plugging in (114). Construct a Lyapunov function as

$$\mathbb{V}_k := f(W_k) + \frac{\alpha C_f M^2}{2} \sum_{m'=1}^M \sum_{k'=k-(M-m'+1)}^{k-1} (k' - k + M - m' + 2) \|\Delta_{k'}^{(m')}\|^2. \quad (116)$$

According to (115), we have

$$\mathbb{E}_{\xi_k} [\mathbb{V}_{k+1}] - \mathbb{V}_k$$

$$\begin{aligned}
&\leq -\frac{\alpha}{2}\|\nabla f(W_k)\|^2 + \alpha^2 L_f \sigma^2 + \frac{\alpha C_f M^2}{2} \sum_{m'=1}^M \sum_{k'=k-(M-m'+1)}^{k-1} \mathbb{E}_{\xi_k} [\|\Delta_{k'}^{(m')}\|^2] \\
&\quad - \frac{1}{4\alpha} \mathbb{E}_{\xi_k} [\|W_{k+1} - W_k + \alpha(\nabla f(W_k; \xi_k) - \nabla f(W_k))\|^2] \\
&\quad + \frac{\alpha C_f M^2}{2} \sum_{m'=1}^M \sum_{k'=k-(M-m'+1)}^k (k' - k + M - m' + 1) \mathbb{E}_{\xi_k} [\|\Delta_{k'}^{(m')}\|^2] \\
&\quad - \frac{\alpha C_f M^2}{2} \sum_{m'=1}^M \sum_{k'=k-(M-m'+1)}^{k-1} (k' - k + M - m' + 2) \mathbb{E}_{\xi_k} [\|\Delta_{k'}^{(m')}\|^2] \\
&\leq -\frac{\alpha}{2}\|\nabla f(W_k)\|^2 + \alpha^2 L_f \sigma^2 + \frac{\alpha C_f M^2}{2} \sum_{m'=1}^M \sum_{k'=k-(M-m'+1)}^{k-1} \mathbb{E}_{\xi_k} [\|\Delta_{k'}^{(m')}\|^2] \\
&\quad - \frac{1}{4\alpha} \mathbb{E}_{\xi_k} [\|W_{k+1} - W_k + \alpha(\nabla f(W_k; \xi_k) - \nabla f(W_k))\|^2] \\
&\quad - \frac{\alpha C_f M^2}{2} \sum_{m'=1}^M \sum_{k'=k-(M-m'+1)}^{k-1} \mathbb{E}_{\xi_k} [\|\Delta_{k'}^{(m')}\|^2] + \frac{\alpha C_f M^2}{2} (M - m' + 1) \sum_{m'=1}^M \mathbb{E}_{\xi_k} [\|\Delta_k^{(m')}\|^2]. \\
&\leq -\frac{\alpha}{2}\|\nabla f(W_k)\|^2 + \alpha^2 L_f \sigma^2 + \frac{\alpha C_f M^2}{2} \sum_{m'=1}^M \sum_{k'=k-(M-m'+1)}^{k-1} \mathbb{E}_{\xi_k} [\|\Delta_{k'}^{(m')}\|^2] \\
&\quad - \frac{1}{4\alpha} \mathbb{E}_{\xi_k} [\|W_{k+1} - W_k + \alpha(\nabla f(W_k; \xi_k) - \nabla f(W_k))\|^2] \\
&\quad - \frac{\alpha C_f M^2}{2} \sum_{m'=1}^M \sum_{k'=k-(M-m'+1)}^{k-1} \mathbb{E}_{\xi_k} [\|\Delta_{k'}^{(m')}\|^2] + \frac{\alpha C_f M^3}{2} \sum_{m'=1}^M \mathbb{E}_{\xi_k} [\|\Delta_k^{(m')}\|^2] \\
&\leq -\frac{\alpha}{2}\|\nabla f(W_k)\|^2 + \alpha^2 L_f \sigma^2 + \frac{\alpha C_f M^2}{2} \sum_{m'=1}^M \sum_{k'=k-(M-m'+1)}^{k-1} \mathbb{E}_{\xi_k} [\|\Delta_{k'}^{(m')}\|^2] \\
&\quad - \frac{\alpha C_f M^2}{2} \sum_{m'=1}^M \sum_{k'=k-(M-m'+1)}^{k-1} \mathbb{E}_{\xi_k} [\|\Delta_{k'}^{(m')}\|^2] + \alpha^3 C_f M^3 \sigma^2 \\
&\quad - \left(\frac{1}{4\alpha} - \alpha C_f M^3 \right) \mathbb{E}_{\xi_k} [\|W_{k+1} - W_k + \alpha(\nabla f(W_k; \xi_k) - \nabla f(W_k))\|^2] \\
&\leq -\frac{\alpha}{2}\|\nabla f(W_k)\|^2 + \alpha^2 L_f \sigma^2 + \alpha^3 C_f M^3 \sigma^2
\end{aligned}$$

where the fourth inequality holds because

$$\begin{aligned}
\sum_{m'=1}^M \mathbb{E}_{\xi_k} [\|\Delta_k^{(m')}\|^2] &= \sum_{m'=1}^M \mathbb{E}_{\xi_k} [\|W_{k+1}^{(m')} - W_k^{(m')}\|^2] = \mathbb{E}_{\xi_k} [\|W_{k+1} - W_k\|^2] \\
&\leq 2\mathbb{E}_{\xi_k} [\|W_{k+1} - W_k + \alpha(\nabla f(W_k; \xi_k) - \nabla f(W_k))\|^2]
\end{aligned} \tag{117}$$

$$\begin{aligned}
& + 2\alpha^2 \mathbb{E}_{\xi_k} [\|\nabla f(W_k; \xi_k) - \nabla f(W_k)\|^2] \\
& \leq 2\mathbb{E}_{\xi_k} [\|W_{k+1} - W_k + \alpha(\nabla f(W_k; \xi_k) - \nabla f(W_k))\|^2] + 2\alpha^2\sigma^2.
\end{aligned}$$

and the last inequality is earned by letting $\alpha \leq \sqrt{\frac{1}{4C_f M^3}}$. Reorganizing the terms yields

$$\frac{\alpha}{2} \|\nabla f(W_k)\|^2 \leq \mathbb{V}_k - \mathbb{E}_{\xi_k}[\mathbb{V}_{k+1}] + \alpha^2 L_f \sigma^2 + \alpha^3 C_f M^3 \sigma^2.$$

Therefore, by telescoping and taking the expectation, we get

$$\begin{aligned}
& \frac{1}{K} \sum_{k=0}^{K-1} \mathbb{E}[\|\nabla f(W_k)\|^2] \leq \frac{2(\mathbb{V}_0 - \mathbb{E}[\mathbb{V}_K])}{\alpha K} + 2\alpha L_f \sigma^2 + 2\alpha^2 C_f M^3 \sigma^2 \quad (118) \\
& \leq \frac{2(f(W_0) - f^*)}{\alpha K} + 2\alpha L_f \sigma^2 + 2\alpha^2 C_f M^3 \sigma^2.
\end{aligned}$$

Letting $\alpha \leq \sqrt{\frac{f(W_0) - f^*}{L_f \sigma^2 K}}$, we obtain that

$$\frac{1}{K} \sum_{k=0}^{K-1} \mathbb{E}[\|\nabla f(W_k)\|^2] \leq 4\sqrt{\frac{(f(W_0) - f^*)L_f \sigma^2}{K}} + \frac{2C_f M^3 (f(W_0) - f^*)}{KL_f}.$$

□